CD300e as a Driver of Immunosuppressive Tumor Microenvironment in Colorectal Cancer

Annica Barizza[1†], Stefania Vassallo[1†], Laura Masatti[1], Silvia Lonardi[2], Mattia Bugatti[2], Sara Coletta[1], Sofia Giacometti[1], Simone Pizzini[1], William Vermi[2], Fabio Munari[3], Nicolò Gnoato[1], Matteo Fassan[4,5], Giulia Nigro[6], Gaya Spolverato[7], Enrica Calura[1], Gaia Codolo[1*]

[1] Department of Biology, University of Padova, 35131 Padua, Italy.

[2] Section of Pathology, Department of Molecular and Translational Medicine, University of Brescia, 25123 Brescia, Italy.

[3] Department of Physics and Astronomy, University of Padova, 35131 Padua, Italy.

[4] Department of Medicine (DIMED), Surgical Pathology Unit, University of Padua, Padua, Italy.

[5] Veneto Institute of Oncology, IOV-IRCCS, Padua, Italy.

[6] Microenvironment and Immunity Unit, INSERM U1224, Institut Pasteur, Paris, France.

[7] Department of Surgical, Oncological and Gastroenterological Sciences (DiSCOG), University of Padua, Padua, Italy

*Corresponding author, email address gaia.codolo@unipd.it

† These authors contributed equally to this work

Keywords

Tumor, CD300e, tumor-associated macrophages, colorectal cancer, immune suppression

Abstract

Tumor-associated macrophages (TAMs) are the predominant immune population within the tumor microenvironment (TME), playing a key role in promoting tumor growth and establishing an immunosuppressive environment that facilitate immune evasion. Here we report that the immune receptor CD300e is highly expressed by TAM in colorectal (CRC) and drives their immunosuppressive and pro-tumorigenic, correlating with reduced expression of MHC-II molecules, essential for antigen presentation. In vitro, CD300e-deficient macrophages exhibit enhanced pro-inflammatory activity and phagocytic capacity, coupled with reduced efferocytosis, suggesting a critical role for CD300e in promoting tumor progression. The depletion of CD300e, in vivo, results in a reduced tumor burden and enhanced survival in CRC mouse models, accompanied by a more robust anti-tumor immune response characterized by increased infiltration of activated CD4+ and CD8+ T cells producing IFN-γ. Our study provides comprehensive insights into the roles of CD300e in myeloid cells in CRC, highlighting its potential as a therapeutic target for reprogramming TAMs to support anti-tumor immunity.

Introduction

Colorectal cancer (CRC) is the most common malignancy of the gastrointestinal tract, and it is the second most common cause of death related to cancer[1,2]. Even though the activation of oncogenic signals in tumor cells due to the genetic and epigenetic alterations significantly contribute to CRC development, therapeutic interventions targeting these pathways gained limited success in patients[3]. Accordingly, emerging evidence in recent years has pointed to a pivotal role of signals coming from the tumor microenvironment (TME) in the development and progression of CRC. The TME refers to a complex biological environment composed by tumor cells together with non-malignant infiltrating cells – including immune cells and stromal cells – and their secreted components, vasculature, and extracellular matrix[3,4]. Notably, a correlation between the density of immune populations composing the TME and CRC clinical course has been reported[5,6], and the Immunoscore system was introduced to define CRC stage based on the density of antitumor T cell subsets in the TME[7,8]. Among immune populations supporting cancer growth in the TME, tumor-associated macrophages (TAMs) are the most abundant[9]. Although macrophages are potentially able to mount a robust anti-tumor response, the profile of TAMs is skewed towards an anti-inflammatory, tumor promoting function as cancer progresses[10,11]. Indeed, TAMs are potent inducers of the process of epithelial to mesenchymal transition (EMT) in cancer cells, they promote tumor invasiveness and metastasis, enhance tumor cell proliferation, stimulate angiogenesis and the remodeling of the extracellular matrix, which is involved in cancer dissemination[12–15]. TAMs are pivotal contributors to the establishment and maintenance of the immunosuppressive milieu within the TME that facilitates cancer immune evasion; primarily through the release of immunosuppressive factors, they can directly or indirectly dampen the antitumor activity of T cells and NK cells in the TME[16]. For instance, they are able to inhibit the recruitment of CD8+ T cells to

the TME, to impair T cell activation and proliferation through inhibitory immune checkpoints, and to induce the recruitment of T regulatory (Treg) cells[17–20].

In CRC, a high infiltration of TAMs in the tumor was correlated with cancer progression and a worse outcome of the disease[19,21], together with resistance to immunotherapies[22]. In recent years, TAMs have emerged as crucial targets for immunotherapy, even though most TAM-targeted therapeutic strategies didn't provide the desired results[22–24]. This prompts a deeper investigation of TAM function in CRC to develop effective treatments able to hijack their tumor-promoting ability.

As it was recently reported, the activation of the immune receptor CD300e is involved in the mechanisms of immune evasion in the context of chronic infections[25]. CD300e is expressed on the surface of myeloid cell subsets, mostly including monocytes and macrophages, both in humans and mice[26–28]. Despite being initially considered as an activating receptor[29], it was shown that the engagement of CD300e in macrophages restrains their ability to induce T cell proliferation, this effect being mediated by an impairment of macrophage antigen presentation ability[30]. In accordance with an immunoregulatory function of CD300e, recent studies reported an association between the upregulation of CD300e and the induction of an immunosuppressive profile on human macrophages[31,32]. These observations position CD300e as a potential player in the modulation of tumor immune responses, and specifically in shaping the function of macrophages in the tumor. Notably, CD300e is upregulated in the tumor tissue of several human cancers, including CRC, and a significant prognostic value of CD300e expression emerged in various tumors, where CD300e represents a risk factor for patients' survival[33,34].

In the present study we revealed the unexplored function of CD300e in shaping the functional profile of TAMs in colorectal cancer. Here, we reveal that CD300e is highly expressed in CRC TAMs with an immunosuppressive phenotype and its expression is associated with the pro-tumor function of TAMs. Furthermore, the expression of CD300e in TAMs exerts a pro-tumoral role by driving the

modulation of the tumor immune environment, impairing the recruitment of effector $CD4^+$ and $CD8^+$ cytotoxic T cells into the TME via inhibition of antigen presentation molecules expression. Consequently, targeting CD300e inhibits CRC progression improving the anti-tumor immune response. Our findings pave the way for a profound understanding of the mechanisms by which CD300e exerts its immunomodulatory function and highlight the receptor as a novel therapeutic target for switching TAMs toward an antitumorigenic phenotype for the treatment of CRC.

Material and Methods

Patients and healthy donors

Surgical resections of tumor (CRC) and normal (NC) colonic tissue were collected from 8 CRC patients who underwent curative-intent surgery, following ethical standards, the Declaration of Helsinki, and national and international guidelines. Written informed consent was obtained from the individual patients, and the Ethical Committee of Padua University Hospital approved the protocol (Protocol Number: P448). Inclusion criteria for enrolled patients were as follows: patients histologically confirmed primary adenocarcinoma of the colon, age >18 years, and provision of written informed consent. Patients with a known history of hereditary colorectal cancer syndrome and patients who had undergone neoadjuvant treatments were excluded. Patients' characteristics are detailed in Table 1.

		CRC patients (n=8)
Age	Median (range), years	74 (65-84)
Sex	Male Female	6 (75%) 2 (25%)
Grade	1 2 3 4	0 5 (62.5%) 3 (37.5%) 0
TNM	I II III IV	0 4 (50%) 4 (50%) 0
Tumor histotype	Adenocarcinoma	8 (100%)

Table 1. Clinicopathological characteristics of CRC patients. CRC: colorectal cancer; TNM: pathological Tumor, Node, Metastasis stage.

Peripheral blood mononuclear cells utilized in this study were derived from buffy coats obtained from healthy blood donors and anonymously provided by the Transfusion Centre of the University Hospital of Padova, as a consequence of voluntary and informed blood donation for transfusions.

Written informed consent for the use of the buffy coats for research purposes was obtained from blood donors by the Transfusion Centre.

Cell lines

MC38 mouse adenocarcinoma cells were cultured in DMEM supplemented with 10% FBS, 100 U/mL penicillin, and 100 µg/mL streptomycin. When ~80% confluence was reached, cells were injected into mice. L929 mouse fibroblast cells were cultured in DMEM supplemented with 10% FBS, 100 U/mL penicillin, and 100 µg/mL streptomycin. L929 conditioned medium was used to differentiate in vitro bone marrow-derived macrophages. Wnt-3a-, R-spondin1- and Noggin-producing cell lines were cultured in DMEM supplemented with 10% FBS, 100 U/mL penicillin, and 100 µg/mL streptomycin, according to datasheet. These cell lines were kindly provided by Prof. Calvin Kuo (Stanford University, R-Spondin-1-producing cells) and Prof. Jeroen den Hertog (Hubrecht Institute, Wnt-3a and Noggin-producing cells).

Mouse experimental models

Animals

Mice were housed at our Institutional Animal Facility. All protocols were approved by the ethical committee of the Italian Ministry of Health (Protocol number 858/2023-PR). Mice were housed in a temperature (22–24°C) and humidity-controlled (50%) colony room, maintained on a 12 h light/dark cycle, with standard food and freely available water and environmental enrichment.

CD300e$^{-/-}$ total knockout mouse model was generated on a C57Bl/6j background at the Transgenic Core Facility of the University of Copenhagen and homozygous litters were obtained at the animal facility of the Department of Biology, University of Padova. Wild-type (CD300e$^{+/+}$) C57Bl/6j mice

were used as controls. Experiments were conducted on age- and sex-matched 8- to 10- week-old mice housed in the same animal facility.

Subcutaneous tumor model and macrophage adoptive transfer

To establish a syngeneic tumor model, a 100 µL tumor cell suspension containing 10^6 MC38 cells in a mixture of phosphate-buffered saline (PBS) and Matrigel™ (Corning, Corning, NY, USA; 1:1 ratio) was subcutaneously (s.c.) engrafted into the right flank of male mice.

For the macrophage adoptive transfer, primary bone marrow-derived macrophages (BMDMs) isolated from CD300e$^{+/+}$ and CD300e$^{-/-}$ mice were polarized towards a tumor-associated macrophages (TAMs) profile with mIL-4 20 ng/ml and mixed with MC38 cells in a ratio of 1:2, and 7.5×10^5 total cells were s.c. injected in CD300e$^{+/+}$ recipient mice, as previously reported[35].

Tumor dimensions were measured once the tumors were palpable. Tumor growth was monitored three times per week with a digital caliper, and tumor volume was calculated using the formula $0.5 \times L \times W^2$, being L and W length and width, respectively. Mice were euthanized on the 21st day after MC38 inoculation or when tumors reached 1.5 cm in diameter. The tumor's final volume was accurately calculated by multiplying length, width, and height (L × W × H).

AOM/DSS-induced colorectal cancer

To induce the development of colitis-associated colorectal cancer, male mice were injected intraperitoneally with a single dose of 10 mg/kg azoxymethane (AOM, Sigma Aldrich, St. Louis, Missouri, USA). Three days later, mice received 2% dextran sodium sulfate (DSS, molecular weight: 36-50 kDa, MP Biomedicals, Irvine, California, USA) in drinking water over 5 days, followed by 16 days of recovery in regular water. This cycle of DSS treatment was repeated two more times, and mice were sacrificed 4 weeks after the last DSS administration. The clinical course of colitis was evaluated by monitoring mice body weight during the course of the experiment, and by checking the presence of diarrhea and blood after DSS cycles.

Tumor and normal colon organoids

Generation of patient-derived organoids

Patient-derived tumor colon organoids (TCO) were generated from surgical resections of CRC patients' primary tumor tissue, as previously reported by Sato et al[36]. Tumor tissue was minced into small pieces (2-4 mm). Tumor fragments were digested in DMEM medium supplemented with 2% FBS, 2 mg/mL Collagenase II (Sigma Aldrich), 100 µg/mL DNAse I (Roche, Basel, Switzerland), 100 U/mL penicillin, and 100 µg/mL streptomycin for 1 hour at 37°C under constant rolling. The obtained cell suspension was filtered through a 70 µm filter, washed in Advanced DMEM/F12 (Gibco, Thermo Fisher Scientific, Waltham, MA, USA) supplemented with 2 mM GlutaMAX (Gibco), 1 mM HEPES (Corning, Corning, NY, USA), 100 U/mL penicillin, and 100 µg/mL streptomycin, and seeded in MatrigelTM (2000 cells/µL).

Patient-derived normal colon organoids (NCO) were generated from colonic crypts obtained from CRC patients' matched normal mucosa. Mucosal tissue was fragmented into small pieces (2-4 mm) and incubated in 3 mM EDTA, 0.5 mM dithiothreitol (DTT) in PBS with 2% FBS for 40 minutes at 4°C, under constant rolling to allow crypt release. Crypt suspension was filtered through a 70 µm filter, washed with Advanced DMEM/F12 supplemented with 2 mM GlutaMAX, 1 mM HEPES, 100 U/mL penicillin, and 100 µg/mL streptomycin, and seeded in MatrigelTM.

Generation of murine organoids

Murine TCO were generated starting from colon tumors of WT mice treated with AOM/DSS (as described previously). At the end of the treatment, mice were sacrificed, colons were collected and opened longitudinally. Colonic tumors were resected, minced into small fragments (2-4 mm) and digested in DMEM supplemented with 2% FBS, 2 mg/mL Collagenase II, 125 µg/mL Dispase II (Sigma Aldrich), 100 µg/mL DNAse I, 100 U/mL penicillin, and 100 µg/mL streptomycin for 45-60 minutes

at 37°C, under constant agitation. After digestion, cell suspension was filtered, washed and seeded in MatrigelTM as described for patient-derived TCO.

Murine NCO were generated from colon crypts of untreated WT mice. After sacrifice, colons were opened longitudinally and cut into 3-5 mm fragments. Crypts were obtained through incubation of colonic fragments in 5 mM EDTA, 0.5 mM DTT in PBS with 100 U/mL penicillin, and 100 µg/mL streptomycin for 20 minutes at room temperature under constant rolling. Crypt suspension was filtered, washed and seeded in MatrigelTM as described for human NCO.

Organoid culture

Organoids were cultured in tumor or normal colon organoid medium, accordingly. Tumor colon medium is composed of advanced DMEM/F12 supplemented with 2 mM GlutaMAX, 10 mM HEPES, 100 U/mL penicillin, 100 µg/mL streptomycin, 20% R-Spondin1 conditioned medium (RCM), 10% Noggin conditioned medium (NCM), 10 mM Nicotinamide (Sigma Aldrich), 1X B27 Supplement (Gibco), 1 mM N-acetyl-L-cysteine (Cayman Chemical, Ann Arbor, Michigan, USA), 50 ng/mL EGF (Corning), 10 µM Y-27632 (ROCK inhibitor, Selleckchem, Houston, TX, USA) 500 nM A83-01 (Tocris Bioscience, Bristol, UK), 3 µM SB202190 (Sigma Aldrich), 100 µg/mL Primocin (Invivogen, San Diego, CA, USA). A 50% of Wnt-3a conditioned medium (WCM) was added to the normal colon organoid medium. Gastrin I (10 Nm, Sigma Aldrich) and Prostaglandin E2 (10 nM, Sigma Aldrich) were added to the medium of both patient-derived TCO and NCO. WCM, RCM and NCM were obtained from Wnt-3a-, R-spondin1-, and Noggin-producing cell lines, respectively. Organoids were passaged 6-7 days after seeding, and then once a week.

Murine TCO-derived epithelial monolayers

Murine tumor cell monolayers were generated on Transwell inserts for 24-well plates (pore size 0.4 µm, Corning) starting from TCO cultures, as reported elsewhere[37]. Organoids were incubated in Cell Recovery Solution (Corning) for 30 minutes on ice, washed with cold PBS and gently pipetted for a

mild mechanical disruption. After washing, organoid fragments were incubated in TrypLE Express (Gibco) diluted 1:2 in PBS for 1 to 3 minutes at 37°C to dissociate organoids to single cells. After washing with Advanced DMEM/F12 supplemented with 2 mM GlutaMAX, 1 mM HEPES, 100 U/mL penicillin, and 100 µg/mL streptomycin, cells were resuspended in tumor organoid medium and seeded on the top of Transwell inserts that were pre-coated with 2% Matrigel in PBS (50000 cells/Transwell in 100 µL of tumor colon organoid medium).

Monocyte purification, macrophages differentiation and polarization

Human monocytes were purified from buffy coats of healthy donors as reported elsewhere[38] or using Pan Monocyte Isolation Kit (Miltenyi Biotec, Bergisch Gladbach, North Rhine-Westphalia, Germany), following the manufacturer's instructions.

Mouse bone marrow cells were isolated to purify monocytes and to differentiate macrophages *in vitro*. Bone marrow cells were obtained by flushing femurs and tibias with RPMI medium supplemented with 10% FBS, 100 U/mL penicillin, and 100 µg/mL streptomycin. Cells were filtered through a 70 µm filter and red blood cells were lysed using BD PharmLyse Lysing Buffer (Becton Dickinson, Franklin Lakes, NJ, USA). Monocytes were purified from bone marrow cells using Monocyte Isolation Kit (BM), mouse (Miltenyi Biotec). To differentiate macrophages, bone marrow cells were seeded in Petri dishes in RPMI medium supplemented with 10% FBS, 100 U/mL penicillin, and 100 µg/mL streptomycin, and 10% conditioned medium obtained from L929 cell line, containing macrophage – colony stimulating factor (M-CSF). Macrophage differentiation was obtained 7 days after seeding. To polarize macrophages *in vitro*, culture medium was removed at day 7 and replaced with RPMI supplemented with 10% FBS, 100 U/mL penicillin, and 100 µg/mL streptomycin, containing 100 ng/mL mIFN-γ (Miltenyi Biotec) or 20 ng/mL mIL-4 (20 Miltenyi Biotec) and 20 ng/mL mIL-13 (Miltenyi Biotec), for 48 hours.

Co-cultures of monocytes/macrophages and organoids

Human monocytes purified from buffy coats were co-cultured together with either patient-derived TCO or NCO. After 3-4 days from passage, organoid culture medium was removed, and 2.5×10^5 monocytes resuspended in DMEM supplemented with 10% FBS, 4 mM HEPES and 50 µg/mL gentamycin were added to each organoid well. After five days of co-culture, monocytes were harvested and analyzed by flow cytometry and qRT-PCR; co-culture supernatants were collected for analysis of cytokine content.

Murine BMDMs were polarized towards an immunosuppressive profile with IL-4 and IL-13 prior to co-culture with murine TCO or NCO. Macrophages were detached with 5 mM Na-EDTA, resuspended in DMEM supplemented with 10% FBS, 100 U/mL penicillin, and 100 µg/mL streptomycin, and added to organoid wells (1.3×10^5 cells/well) after organoid medium removal (4-5 days after organoid passage). After 48 h, macrophages and organoids were separately harvested and analyzed by qRT-PCR; co-culture supernatants were collected for analysis of cytokine content.

A 2D co-culture system of BMDMs polarized with mIL-4 and mIL-13 and TCO-derived monolayers was performed. After monolayers completely formed (48 h after cell seeding), culture medium was removed from the bottom compartment of Transwells and the plate was inverted upside-down. Macrophages (5×10^4 cells/Transwell) resuspended in DMEM supplemented with 10% FBS, 100 U/mL penicillin, and 100 µg/mL streptomycin were seeded on the bottom side of the Transwell. After macrophages adhered to the insert, the plate was reverted and both top and bottom compartments of Transwell inserts were filled with DMEM supplemented with 10% FBS, 100 U/mL penicillin, and 100 µg/mL streptomycin. Macrophages and TCO-derived monolayers were kept in co-culture for 48 h.

Western blot

Wester blot was performed as reported elsewhere[39]. Briefly, human HC and CRC tissue from surgical resections of CRC patients were lysed in RIPA buffer (50 mM Tris-HCl, pH 7.4, 150 mM NaCl, NP-40 1%, Na-deoxycholate 0.5%, SDS 0.1%, 2 mM EDTA, 50 mM NaF, 1 mM Na3VO4, 1 mM EGTA, 2% PMSF) with protease inhibitor cocktail (Millipore, Burlington, MA, USA) using TissueLyser II (Qiagen, Hilden, North Rhine-Westphalia, Germany) to homogenize the tissue. Proteins were quantified by BCA protein assay kit (Thermo Fisher Scientific, Waltham, MA, USA) according to the manufacturer's instructions. Thirty µg of total proteins from each sample were resuspended in NuPAGE LDS loading buffer (Novex, Thermo Fisher Scientific) supplemented with 50 mM DTT and denatured for 5 minutes at 100°C. Proteins were electrophoretically separated by SDS-PAGE in a NuPAGE Bis-Tris 4-12% polyacrylamide gel (Novex, Thermo Fisher Scientific), and then transferred on PVDF membranes (Millipore). Membranes were subsequently blocked with 5% milk in Tris-buffered saline (TBS, 50 mM Tris-HCl pH 7.6, 150 mM NaCl) containing 0.1% Tween20 (Sigma-Aldrich), and antigens were revealed using the following antibodies: rabbit anti-vinculin antibody (1:5000, clone 42H89L44, Invitrogen, Waltham, MA, USA) and rabbit anti-human CD300e polyclonal antibody (1:1000, Sigma Aldrich). After washing with TBS plus 0.1% Tween20, PVDF membranes were incubated for 1 h at room temperature with horseradish peroxidase-conjugated anti-rabbit IgG secondary antibody (Millipore). Blots were developed with enhanced chemiluminescence substrate (EuroClone, Pero, Italy), and protein bands were detected using ImageQuant LAS 4000 (GE Healthcare, Chicago, IL, USA).

Flow cytometry

Human macrophages

After 5 d of co-culture with NCO or TCO, human monocyte-derived macrophages were harvested from culture wells using 5 mM Na-EDTA in PBS and incubated for 10 minutes at room temperature with Human Fc Block (BD Biosciences, Franklin Lakes, NJ, USA) to saturate Fc receptors. Cells were stained with the following antibodies: APC anti-MHC-II (clone L243, eBiosciences, San Diego, CA, USA), BB515 anti-CD206 (clone 19.2, eBiosciences), PE-Cy7 anti-CD86 (clone IT2.2, eBiosciences) and PE anti-CD300e (clone UP-H2, Invitrogen). The fixable cell viability dye eFluor780 (eBiosciences) was used to exclude dead cells from the analysis. Cells were washed with PBS and acquired with the flow cytometer.

Murine blood and bone marrow cells

Peripheral blood from 8-week-old mice was collected in EDTA-treated tubes and incubated with BD PharmLyse Lysing Buffer (BD Biosciences) to lyse erythrocytes. Blood cells or bone marrow cells, isolated as previously described, were incubated for 10 minutes at 4°C with TruStain FcXTM PLUS (clone S17011E, BioLegend, San Diego, CA, USA) to saturate Fc receptors. Cells were then stained with the following antibodies: FITC anti-mouse CD45 (clone 30-F11, BioLegend), BV785 anti-mouse Ly6C (clone HK1.4, SONY, San Jose, CA, USA), PE-Cyanine7 anti-mouse Ly6G (clone 1A8, SONY), BV421 anti-mouse CD11b (clone M1/70, SONY), BV605 anti-mouse NK-1.1 (clone PK136, SONY), APC-Cyanine7 anti-mouse CD3e (clone 145-2C11, SONY), PerCP-Cyanine5.5 anti-mouse CD8a (clone 53-6.7, SONY), APC-conjugated anti-mouse CD4 (clone GK1.5, SONY), PE anti-mouse CD19 (clone 1D3/CD19, SONY). The fixable viability dye Zombie AquaTM (BioLegend) was used to exclude dead cells from the analyses.

Subcutaneous and colonic tumors

Subcutaneous tumors were isolated and cut into small pieces of 2-4 mm in Petri dishes. The minced tissues were transferred into gentleMACS Tubes (Miltenyi Biotec) containing DMEM with 1 mg/mL collagenase IV (Sigma-Aldrich) and 0.5 mg/mL Dnase I. gentleMACS Tubes were attached onto a

gentleMACS Octo Dissociator (Miltenyi Biotec) and tumors were maintained for 40 minutes at 37°C under continuous rotation. The resulting cell suspension was filtered through a 70 µm strainer and incubated with TruStain FcX PLUS. To characterize tumor-infiltrating myeloid lineage, cells were incubated with the following antibodies: FITC anti-mouse CD11c (clone N418; BioLegend), PE/Dazzle 594 anti-mouse I-A/I-E (clone M5/114.15.2; BioLegend), PerCP/Cyanine5.5 anti-mouse H-2Kb/H-2Db (clone 28-8-6; BioLegend), PE-Cyanine7 anti-mouse F4/80 (clone BM8; BioLegend), Alexa Fluor 700 anti-mouse Ly6G (clone 1A8; BioLegend), BV421 anti-mouse Ly6C (clone HK1.4; BioLegend), BV510 anti-mouse CD3 (clone 145-2C11, BioLegend), BV510 anti-mouse CD19 (clone 6D5, BioLegend), BV510 anti-mouse NK-1.1 (clone PK136, BioLegend), BV650 anti-mouse CD274 (PD-L1; clone 10F9G2, BioLegend), BV785 anti-mouse CD11b (clone M1/70, BioLegend). The fixable cell viability dye eFluor780 (eBiosciences) was used to exclude dead cells. To characterize tumor-infiltrating lymphoid lineage, cells were incubated with the following antibodies: FITC anti-mouse CD62L (clone MEL-14; BioLegend), PE anti-mouse CD44 (clone IM7; BioLegend), APC anti-mouse CD25 (clone 3C7; BioLegend), Alexa Fluor 700 anti-mouse CD8a (clone QA17AO7; BioLegend), APC-Cyanine7 anti-mouse CD3e (clone 145-2C11; BioLegend), BV421 anti-mouse CD279 (PD-1; clone 29F.1A12; BioLegend), BV605 anti-mouse CD69 (clone H1.2F3; BioLegend), BV650 anti-mouse CD4 (clone RM4-5; BioLegend), BV785 anti-mouse CD11b (clone M1/70; BioLegend). The fixable viability dye Zombie AquaTM was used to exclude dead cells.

T cells isolated from subcutaneous tumor and lymph nodes

Tumor-infiltrating lymphocytes were purified from dissociated MC38-derived tumors using the EasySep Mouse T Cell Isolation Kit (STEMCELL Technologies, Vancouver, Canada), according to the manufacturer's instructions. Local lymph nodes of MC38 tumor-bearing mice and mesenteric lymph nodes of AOM/DSS-treated mice were collected, placed on a 70 µm filter and mechanically disrupted using a syringe plunger.

0.5×10^6 tumor-infiltrating lymphocytes, as well as T cells isolated from local and mesenteric lymph nodes, were seeded in 48-well plate pre-coated with Purified anti-mouse CD3 (1:50 in PBS; clone 145-2c11; BioLegend) in RPMI supplemented with 10% FBS, 100 U/mL penicillin, and 100 µg/mL streptomycin, containing Ultra-LEAF Purified anti-mouse CD28 antibody (1:1000; clone 37.51; BioLegend). After an overnight stimulation, BD GolgiStop Protein Transport Inhibitor (Containing Monensin) (1:10 in RPMI, 10% FBS, 100 U/mL penicillin, 100 µg/mL streptomycin; BD Biosciences) was added and maintained for 5 h. Cells were incubated with TruStain FcXTM PLUS, then the following antibodies were added: PE anti-mouse CD19 (clone 1D3/CD19, BioLegend), PerCP/Cyanine5.5 anti-mouse CD8a (clone 53-6.7; BioLegend), APC anti-mouse CD3 (clone 145-2C11; BioLegend), BV650 anti-mouse CD4 (clone RM4-5; BioLegend). The fixable viability dye Zombie AquaTM (BioLegend) was used to exclude dead cells. For IFN-ɣ detection, cells were fixed with 3.6% formaldehyde (Sigma-Aldrich), permeabilized with permeabilization buffer (0.2% saponin, 1% FBS, in H2O MilliQ), and stained with FITC anti-mouse IFN-ɣ (clone XMG1.2; BioLegend). Flow cytometry data were analyzed using FlowJo version 10.3 (Tree Star, Ashland, OR, USA).

Histology

Hematoxylin and Eosin

Hematoxylin and Eosin staining of liver, spleen, and colon samples were performed on formalin-fixed paraffin embedded (FFPE) tissue sections. Slices were hydrated, stained with Mayer's hematoxylin (Bio-Optica, Milan, Italy) and Eosin Y 1% aqueous solution (Bio-Optica) and dehydrated in ethanol. Images were acquired with the Leica DM6 microscope (Leica Biosystems, Nussloch, Germany) using LasX software.

Immunohistochemistry

Immunohistochemistry on matched NC and CRC tissues from CRC patients was performed in collaboration with the University of Brescia. FFPE tissue sections were sequentially immunostained as described previously30. Briefly, MHC-II (clone V1030, dilution 1:500; Biomeda, Foster City, CA, USA) was revealed using Novolink Polymer (Leica Biosystems). Slides were then decolored using ethanol and the previous antibody was stripped using a β-mercaptoethanol/SDS solution in a waterbath preheated at 56°C. Double immunohistochemistry using CD163 (clone 10D6, dilution 1:80; Thermo Scientific) and CD300e (Sigma Aldrich) was performed on the same sections. The first was revealed using Mach4AP Polymer (Biocare Medical, Concord, CA, USA) and Ferangi Blue as a chromogen, the second was revealed using Novolink Polymer (Leica Biosystems) followed by Diaminobenzidine (DB). The two digital slides were synchronized using ImageScope and pictures of the same area were taken to highlight the same cells sequentially stained for MHC-II/CD300e and CD163. Cells were quantified by optical count using the ImageScope count tool.

RNA extraction and qRT-PCR

Total RNA was extracted with TRIzol reagent (Thermo Fisher) according to the manufacturer's protocol. When working with human or murine colon tissues, the tissue was first disrupted using TissueLyser II (Qiagen). RNA was quantized using a NanoDrop 1000 spectrophotometer (NanoDrop, Wilmington, DE, USA). One µg of total RNA was retrotranscribed using the High-Capacity cDNA Reverse Transcription Kit (Applied Biosystems, Waltham, MA, USA), following the manufacturer's instructions. Five ng of cDNA was used in qRT-PCR reaction (fifteen ng when working with tissues) performed with PowerUp SYBR Green master mix (Thermo Fisher Scientific). qRT-PCR was performed in QuantStudio5 Real-Time PCR System (Thermo Fisher Scientific) according to the following cycle: 95°C for 5 min, 95°C for 15 s, 60°C for 1 min, for 40 cycles. Experiments were

performed with at least three technical replicates. For each sample, data were normalized to the endogenous reference genes β-actin and 18S. Sequence of primers used are listed as follows.

Gene	Primer	Sequence (5'->3')
hβ-actin	Forward	TGAGATGCGTTGTTACAGGA
	Reverse	ACGAAAGCAATGCTATCA
hCD300e	Forward	GGGAGGTGTTGACCCAAAAT
	Reverse	AGGACCACGAGCAGGAAGT
hMHC-II	Forward	AGGCAGCATTGAAGTCAGGT
	Reverse	ATTCTGAATCAGGCCTGTGG
hCIITA	Forward	GGTCCAGGGTTTGAGTTCAT
	Reverse	TGATTTGGGGTGGCTTGTTA
m18S	Forward	GTAACCCGTTGAACCCCATT
	Reverse	CCATCCAATCGGTAGTAGCG
mβ-actin	Forward	GATTACTGCTCTGGCTCCTAGC
	Reverse	GACTCATCGTACTCCTGCTTGC
mCD300e	Forward	TTCCAGCCACAACTCCTACACTC
	Reverse	GTACTAATCCTCAGGTTCTGCCCAG
mCD38	Forward	GTGGAGACCCTAGTACTTCT
	Reverse	GAACACAGTAATAGGGTTGTTG
mCD86	Forward	CATGGGCTTGGCAATCCTTA
	Reverse	AAATGGGCACGGCAGATATG
mMHC-II	Forward	TTTGCTTTCTGAAGGGGGCA
	Reverse	TCGCCCATGAACTGGTACAC
miNOS	Forward	CGAAACGCTTCACTTCCAA
	Reverse	TGAGCCTATATTGCTGTGGCT
mTNF-α	Forward	TCAAGTGGCATAGATGTGGAAGAA
	Reverse	TGGCTCTGCAGGATTTTCATG
mEGR2	Forward	CAGACTGGTTGGAGGAGAAATC
	Reverse	AATGTTGATCATGCCATCTCC
mCD206	Forward	CCTCTGGTGAACGGAATGAT
	Reverse	CTTCCTTTGGTCAGCTTTGG
mARG1	Forward	CATTTGGGTGGATGCTCACA
	Reverse	TGGTACATCTGGGAACTTTCCTTT
mCD163	Forward	CAGACTGGTTGGAGGAGAAATC
	Reverse	CAGCTTCCAGAGACAAGTCA
mTGF-β	Forward	ACCAACTATTGCTTCAGCTTCAGCTCCAC
	Reverse	GATCCACTTCCAACCCAGGTC
mTWIST1	Forward	AGCGGGTCATGGCTAACG
	Reverse	GGACCTGGTACAGGAAGTCGA
mTWIST2	Forward	GCTACAGCAAGAAATCGAGC
	Reverse	GCTGAGCTTGTCAGAGGGG
mSNAIL	Forward	TGTCTGCACGACCTGTGGAAAG
	Reverse	CTTCACATCCGAGTGGGTTTGG
mZEB1	Forward	ATTCAGCTACTGTGAGCCCTGC
	Reverse	CATTCTGGTCCTCCACAGTGGA

mZEB2	Forward	ACGTCAGTCCGTCCCCAGGTT
	Reverse	ACGTCAGTCCGTCCCCAGGTT
mVIMENTIN	Forward	CCCTGAACCTGAGAGAAACTAAC
	Reverse	GGTCATCGTGATGCTGAGAAG
mMMP9	Forward	GATCCCCAGAGCGTCATTC
	Reverse	CCACCTTGTTCACCTCATTTTG

Table 2: List of human and mouse primers used for qPCR.

RNA sequencing

RNA extracted from mouse monocytes or macrophages was analyzed with 2100 Bioanalyzer (Agilent Technologies, Santa Clara, California, USA) to assess RNA quality and integrity. Samples were used only if the RNA integrity number (RIN) was higher than 7. Library construction and sequencing were performed by the NGS Facility at the University of Padova. RNA sequencing libraries were constructed using Stranded mRNA Prep kit (Illumina, San Diego, CA, USA) and the sequencing was performed on a NovaSeq 6000 instrument (Illumina), using NovaSeq 6000 S4 Reagent Kit v1.5 300 cycles (Illumina). Reads from RNAseq data were mapped with RSEM software (genome sequence GRCm39, annotations from Ensembl version 109.149)[40], and transcript abundances were estimated (RSEM v1.3.1). Transcripts with less than 10 counts in at least 60% of samples per class were filtered out. Differential expression was computed using edgeR (version 3.42.4). Transcripts with a corrected p-value (q-value) <0.05 were considered differentially expressed. Gene Ontology pathway enrichment analysis of differentially expressed genes was performed through the function enrichGO of the R package clusterProfiler (version 4.8.3)[41,42].

ELISA assay

Cytokine content in co-culture supernatants was evaluated with ELISA kits specific for human IL-6 (Thermo Fisher) and IL-10 (Thermo Fisher), following the manufacturer's instructions.

Phagocytosis assays

Phagocytic ability of macrophages was assessed after coculture with TCO using Zymosan BioParticles™ (Invitrogen) or MC38 cells. Since phagocytosis was evaluated at the confocal microscope, both organoids and macrophages in co-culture were seeded on a round coverslip inserted in the well plate.

Zymosan BioParticles™ and control uncoated microspheres

After 48 hours of co-culture, organoids in Matrigel™ were removed from the wells and macrophages were incubated for 30 minutes at 4°C with DMEM supplemented with 0.2% BSA (starvation medium). Cytocalasin D was added to the starvation medium in negative control wells. After the starvation, macrophages were incubated at 37°C with Zymosan A BioParticles™, or control bioparticles non functionalized, in a 5:1 (Zymosan:macrophage) ratio, in starvation medium. Cytocalasin D was maintained in negative control wells. After 1 h, macrophages were directly fixed with 4% paraformaldehyde (PFA) for 20 minutes and permeabilized in 0.2% Triton X-100 in PBS for 30 minutes at room temperature. Cells were blocked in 1% BSA, 0.3% Triton X-100 for 30 minutes at room temperature and stained with anti-F4/80 (dilution 1:50, clone BM8, Invitrogen) overnight at 4°C. Alexa Fluor 488-conjugated goat anti-rat secondary antibody (dilution 1:1000, Invitrogen) was incubated for 1 h at room temperature, and DAPI was used counterstain cell nuclei. Glass slides were mounted using ProLong Diamond Antifade Mountant (Invitrogen) and images were acquired at a Zeiss LSM900 (Carl Zeiss, Milan, Italy) confocal microscope. Images were analyzed using ImageJ software.

MC38 cells

Macrophages and MC38 cells were stained with Vybrant DiO (Invitrogen) and Vybrant DiD (Invitrogen), respectively, according to the manufacturer's instructions. After starvation as previously described, macrophages were incubated with either live or apoptotic MC38 to evaluate

phagocytosis and efferocytosis, respectively. Live MC38 were resuspended in starvation medium and incubated with macrophages at a 3:1 ratio (MC38:macrophages) for 2 h at 37°C. To induce apoptosis, MC38 were put at 56°C for 30 min and then incubated with 20 µM Staurosporin for 2 h at 37°C. Apoptosis induction was evaluated at the flow cytometer using Annexin V/PI staining Kit (Invitrogen), and apoptotic MC38 cells were incubated with macrophages in starvation medium at a 3:1 ratio. After incubation, non-engulfed MC38 cells were removed with several washes in PBS and macrophages were fixed with 4% PFA. Mounting and image acquisition was performed as described in the previous paragraph.

FITC-dextran based permeability assays

The epithelial integrity of murine colon organoids and TCO-derived monolayers co-cultured with macrophages was assessed by evaluating the permeability to 4 kDa FITC-dextran, (FD4, Sigma Aldrich). After 48 h of co-culture with macrophages, murine colon organoids were incubated with 2.5 FD4 for 1 h at 37°C in the dark. Following at least three washes with PBS, images were recorded using a Leica SP5 inverted confocal microscope (Leica Biosystems). Concerning TCO-derived monolayers, FD4 (1 mg/mL) was added to the top compartment of each Transwell insert and incubated at 37°C for 1 h. After incubation, the fluorescence intensity of FD4 (excitation: 483 nm, emission: 530 nm) was measured in the bottom compartment using Infinite M1000 Pro plate reader (Tecan, Männedorf, Switzerland).

Measurement of TEER

Measurement of transepithelial electrical resistance (TEER) across TCO-derived monolayers after 48 h of co-culture with macrophages was performed using an EVOM Manual TEER meter (World Precision Instruments, Sarasota, Florida, USA), according to the manufacturer's instructions.

Statistical analyses

Statistical analyses were performed on GraphPad Prism 8.0 software using one-way or two-way analysis of variance (ANOVA) followed by Šídák's multiple comparisons test or Tukey's test, as appropriate. For two-group comparison, two-tailed Student's t tests were employed. All data are represented as mean ± standard deviation (SD), unless otherwise stated, and differences between groups were considered statistically significant for $p<0.05$. *$p\leq0,05$; **$p\leq0,01$; ***$p\leq0,001$; ****$p\leq0,0001$.

Results

Tumor-Induced CD300e Expression Correlates with MHC-II Downregulation in Macrophages

The expression of CD300e was reported in human CRC tissue by scRNA-seq mapping and protein analysis[43,44]; moreover, the majority of TAM in CRC show an immunosuppressive profile characterized by a low expression of MHC-II molecules[45]. Thus, due to the reported role of CD300e in impairing the expression of MHC-II molecules on macrophages[25] and to the fact that MHC-II downmodulation is a common evasion mechanism in CRC, we investigated the relationship of CD300e and MHC-II expression in tumor-infiltrating macrophages in matched normal colon mucosa (NM) and CRC mucosa (CRC). Tumor mucosa showed a higher expression of CD300e with respect to the matched normal one (Figure 1A and B), and reduced expression levels of MHC-II (Figure 1C). Interestingly, the master regulator of MHC-II transcription, MHC class II Transactivator (CIITA), was significantly downmodulated, as well, in the CRC tissue compared to matched normal tissue (Figure 1D). Of note, histological analysis highlighted that the increased CD300e expression in CRC was attributable to an increased infiltration of $CD163^{+}$ macrophages expressing CD300e. Importantly, the proportion of $CD300e^{+}/MHC\text{-}II^{low}$ macrophages is significantly higher in the tumor tissue with respect to the matched normal mucosa (Figure 1E).

To better understand if CD300e is indeed upregulated in the context of CRC, an *in vitro* setting was exploited to recapitulate the interaction between TAMs and CRC epithelium. Tumor colon organoids (TCO) and normal colon organoids (NCO) were derived from matched tumor tissue and normal colonic mucosa patients and co-cultured with human monocytes (Figure 1F). After 5 d, monocytes acquired a macrophage-like phenotype; the exposure to TCO induced an anti-inflammatory profile characterized by an increased expression of CD300e (Figure 1G) and decreased expression of MHC-II and CD86 paralleled by a higher expression of the anti-inflammatory marker CD206, compared to monocytes-derived macrophages (MDMs) exposed to NCO (Figure 1H and I). Moreover, MDMs co-

cultured with TCO expresse and produced higher amounts of the pro-tumor cytokines TGF-β, IL-6 and IL-10 (Figure 1I). These findings indicate that colorectal cancer epithelium can drive the upregulation of CD300e on macrophages, which is associated with a decrease in MHC-II expression and an anti-inflammatory, pro-tumorigenic profile.

CD300e shapes the profile of macrophages and impacts the interaction between the tumor epithelium and macrophages

To determine whether CD300e directly regulates the macrophage phenotype, we established a systemic *cd300e* deficient mouse (Figure S1A); we choose a total KO model since the receptor is specifically expressed by monocytes/macrophages. In CD300e$^{+/+}$ tissues the receptor is mainly expressed in blood, bone marrow (BM), liver, heart, muscle, lymph nodes, lung and spleen as these tissues are those in which monocytes and macrophages, the cells expressing CD300e, are mainly represented (Figure S1B). The efficient deletion of CD300e was confirmed assessing its expression in different tissues (Figure S1C); moreover, the deletion of the receptor doesn't impact on blood and bone marrow leukocyte populations in both male and female mice (Figure S1D and E) as well as on peritoneal macrophages profile (Figure S1F). No differences between CD300e$^{+/+}$ and CD300e$^{-/-}$ mice were detected from histological analysis (Figure S1G). Extremely limited information is available regarding CD300e function in mice[26]. As a preliminary analysis to investigate the specific function of CD300e in mouse monocytes/macrophages in physiological conditions, the transcriptomes of CD300e$^{+/+}$ and CD300e$^{-/-}$ monocytes from BM were compared by RNAseq. Interestingly, several genes resulted to be differentially expressed in CD300e KO monocytes compared to WT, either significantly up- or down-regulated (Figure S1H). Among the most deregulated pathways there are those associated to antigen presentation complex binding, the immune receptor activity, cytokine binding and chemokine activity (Figure S1I). The analysis of

differentially expressed genes between CD300e$^{+/+}$ and CD300e$^{-/-}$ monocytes, revealed several genes of the MHC class II locus were significantly upregulated in CD300e$^{-/-}$ monocytes (H2-Ab1, H2-Aa, H2-Eb1, CD74), as well as positive regulators of antigen presentation machinery (IFNGR1, IFNGR2, IFNAR1), genes with immunostimulatory, proinflammatory function (e.g. TNFRSF1B, IL17RA, CCR7) and related to phagocytosis process (TLR6, CD180, STAB2, CD36). Genes that were most significantly downregulated in CD300e$^{-/-}$ monocytes share an immunosuppressive function, some of them being reported as positive regulators of the protumor function of TAMs, such as CCL2[46] and TREM2[47] (Figure S1J). This suggests a potential effect of CD300e on the latter, as it has already been recently reported in human monocytes[30].

To define the role of CD300e in determining the functional profile of tumor-associated macrophages (TAMs) in colorectal cancer and the interactions between macrophages and colorectal tumor epithelium, we adopt a co-culture system using bone marrow-derived macrophages (BMDMs) and murine tumor colon organoids (TCOs) to mimic the interaction between TAMs and colorectal cancer epithelium in a simplified yet physiologically relevant context. We first compared the profile of CD300e$^{+/+}$ and CD300e$^{-/-}$ differentiated and polarized BMDM, and we didn't notice substantial differences (Figure S2A and B).

For the co-culture experiments we used IL-4/IL-13 polarized macrophages to mimic the anti-inflammatory profile acquired by MDM once they reach the tumor site becoming TAM, which were reported to induce cancer cell growth and invasion in vitro . After 48 h, CD300e$^{+/+}$ macrophages showed an increased expression of CD300e mirrored by a significant downmodulation of MHC-II, recapitulating what observed in human; interestingly, CD300e$^{-/-}$ cells displayed an increased expression of MHC-II compared to CD300e$^{+/+}$ (Figure 2A and B). RNAseq analysis on BMDM after 48 h of co-culture with TCO revealed a general more pronounced pro-inflammatory/immunostimulating profile in KO macrophages compared to WT (data not shown).

These data were confirmed by qPCR, revealing that the absence of CD300e led to an increase in the expression of several pro-inflammatory genes and decreased of anti-inflammatory one (Figure 2B). Interestingly, this is not recapitulated in macrophages co-cultured with HCO, suggesting that CD300e has a role in shaping macrophages' profile specifically in the tumor context (Figure S3).

The phagocytosis of tumor cells by macrophages serves as an anti-tumor mechanism, though tumor cells may evade by expressing anti-phagocytic signals. Additionally, phagocytosis is vital for activating adaptive anti-tumor immunity, as macrophages present tumor antigens to $CD4^+$ T cells[49,50]. After 48 h of co-culture with TCO $CD300e^{-/-}$ cells exhibited a higher ability to phagocytose zymosan coated beads compared to $CD300e^{+/+}$ counterpart, as demonstrated by the increased number of internalized fluorescent particles (Figure 2C); whereas both $CD300e^{+/+}$ and $CD300e^{-/-}$ macrophages displayed reduced phagocytic capacity when exposed to control uncoated microspheres (Figure S4A). The $CD300e^{-/-}$ cells confirmed their increased phagocytic activity also when exposed to tumor cells (Figure 2 D). These data suggest a role for CD300e in shaping the immunosuppressive phenotype of macrophages within the tumor tissue. The presence of dead cells in the TME can induce an immunosuppressive state in macrophages, and efferocytosis (the phagocytosis of apoptotic cells) within tumor tissue is considered characteristic of a pro-tumoral function of infiltrating macrophages[51,52]. The hypothesis that receptor activation in tumor macrophage associates to a functional profile implicated in sustaining tumor growth was supported by the fact that $CD300e^{+/+}$ macrophages were highly efferocytic compared to $CD300e^{-/-}$ cells after 48 h of co-culture with TCO (Figure 2E). On the contrary, macrophages co-cultured together HCO didn't display different phagocytic capacity (Figure S4B, C and D), highlighting the relevance of the presence of CD300e activating factor(s) specifically associated to pathological conditions.

These findings suggest that CD300e modulates macrophage function within the tumor microenvironment, particularly influencing their inflammatory profile and phagocytic activity[53,54].

CD300e promotes the EMT process mediated by macrophages and increases intestinal epithelium permeability

Since in the tumor context the presence of CD300e impacts on macrophages functional profile, characterized by a higher expression of anti-inflammatory markers and an increased efferocytic capacity, we then evaluated the effect of CD300e$^{+/+}$ and CD300e$^{-/-}$ macrophages on tumor colon organoids. One of the major and most studied mechanisms by which TAMs promote tumor progression is the induction of epithelial to mesenchymal transition (EMT)[14]. The effect of the lack of CD300e on macrophage-mediated induction of EMT in TCO was investigated, revealing a decreased expression of TWIST1 and TWIST2, ZEB1, SNAIL and Vimentin in TCO after 48 h of co-culture with CD300e$^{-/-}$ macrophages (Figure 3A).

The process of EMT leads to a progressive disruption of cell-cell junctions due to the acquisition of a mesenchymal phenotype by tumor cells, leading to an increase in the epithelial permeability[14]. According to EMT, the tumor intestinal epithelium resulted to be less permeant to dextran-FITC when co-cultured with macrophages lacking CD300e expression (Figure 3B); whereas no effect on intestinal epithelium permeability was observed in HCO in the presence of CD300e$^{+/+}$ or CD300e$^{-/-}$ macrophages (Figure S5), confirming that the receptor shapes macrophages' profile in tumor context and not in the physiological one. This was also confirmed in tumor epithelial monolayers derived from TCO co-cultured with CD300e$^{+/+}$ or CD300e$^{-/-}$ macrophages, as demonstrated by dextran-FITC permeability and transepithelial electrical resistance (TEER) measurements (Figure 3C). These results suggest that CD300e is involved in the in TAM-mediated EMT process, mirrored by increased epithelial permeability and compromised intestinal integrity.

CD300e supports the colitis-associated colon cancer development

To define whether CD300e has a role in the development of CRC *in vivo*, we adopted a colitis-associated colorectal cancer model based on azoxymethane (AOM) and dextran sodium sulfate (DSS) treatment[55]. The monitoring of mice weight during treatment revealed that the most dramatic weight loss was observed during the first round of DSS administration; however, the lack of CD300e appeared to mitigate the effect of DSS colitis, as CD300e$^{-/-}$ underwent a smaller loss of weight compared to CD300e$^{+/+}$ animals. No significant differences, and even less dramatic weight loss, were observed during the second and third cycles of DSS administration; nevertheless, the weight of CD300e$^{-/-}$ mice tendentially showed a reduced loss compared to the initial weight (Figure 4A). Of note, the weight of CD300e$^{+/+}$ and CD300e$^{-/-}$ mice at the beginning of the AOM/DSS treatment was equal (Figure S6B). These observations suggest a detrimental effect of CD300e in the response to DSS treatment in mice. Importantly, a higher mortality rate was observed in CD300e$^{+/+}$ animals during the experimental period, with mice dying most frequently during the first cycle of DSS administration; none of CD300e$^{-/-}$ mice died during AOM/DSS treatment (Figure 4B).

Colon shortening is one of the massive effects of DSS treatment and is due to the defective repair of the colonic mucosa after DSS-induced damage. Notably, CD300e absence resulted in longer colons after AOM/DSS treatment compared to CD300e$^{+/+}$ animals (Figure 4C), suggesting that CD300e lack might be protective for DSS-induced damage in the colon or favor epithelial repair, corroborating what observed in Figure 3B and C. This is also confirmed by the fact that colon length in control CD300e$^{+/+}$ and CD300e$^{-/-}$ mice was equal (Figure S6C).

Compared to CD300e$^{+/+}$ mice, macroscopic analysis of CD300e$^{+/+}$ colons showed a significant decrease in the number of neoplastic lesions, as well as a reduced tumor area (Figure 4D). Expression analysis within adenomas revealed a more pronounced immunosuppressive/pro-tumoral profile in CD300e$^{+/+}$ mice (Figure 4E).

Of note, T cells isolated from mesenteric lymph nodes showed similar proportion of $CD4^+$ and $CD8^+$ T cells in $CD300e^{+/+}$ and $CD300e^{-/-}$ mice (Figure S6D), with a significantly higher percentage of activated Th1 and Tc1 producing IFN-γ in $CD300e^{-/-}$ (Figure 4F), suggesting that the lack of the receptor facilitates the development of an anti-tumor immune response. No differences were detected in control mice (Figure S6E).

Lack of CD300e impact the tumoral immune landscape

To investigate whether CD300e has a role in modulating the profile of immune cells infiltrating tumor environment, we adopt a CRC subcutaneous tumor model injecting MC38 colon cancer cell line into $CD300e^{-/-}$ and $CD300e^{+/+}$ mice; this model is known to depend on the function of macrophages infiltrating the tumor[56]. MC38 tumor increasingly grew in $CD300e^{+/+}$ mice, while it was significantly attenuated in $CD300e^{-/-}$ mice (Figure 5A and B), consistently to what observed in AOM/DSS CRC model. We then examined by flow cytometry the immune infiltrate of MC38 tumors in $CD300e^{+/+}$ and $CD300e^{-/-}$ mice 21 days after tumor injection (gating strategy is shown in Figure S7A); total $CD11b^{hi}$ myeloid cells were less represented in $CD300e^{-/-}$ infiltrates (Figure S7B), and this was due to a decreased number of infiltrating neutrophils (Figure 5C), and also of monocytes and macrophages (Figure 5D and E). Despite the reduced infiltration of myeloid cells in $CD300e^{-/-}$ mice, both macrophages and monocytes infiltrating tumors displayed higher expression of MHC-II and MHC-I molecules and reduced expression of the immunosuppressive molecule PD-L1 (Figure 5F and Figure S7C), suggesting that CD300e deficiency may impact the myeloid infiltrate.

Increase of MHCII expression often accompanies with recruitment of activated T lymphocytes; our results showed an increase in the proportion of CD4+ T and CD8+ T cells in tumors after CD300e deletion, despite not significant (Figure 5G; gating strategy detailed in Figure S8), which express significantly less PD-1 (Figure 5H). In addition, $CD300e^{-/-}$ infiltrates contained increased proportion

of activated T cells (Figure S9A and B). Detailed analysis of T cells revealed that GZMB and perforin levels were slightly more abundant in CD300e$^{-/-}$ tumors, although not reaching significance (Figure 5I), while IFN-γ was strongly produced by CD8^{+} and CD4^{+} T cells infiltrating CD300e$^{-/-}$ tumors (Figure 5J); increased IFN-γ-producing T cells were also detected in mesenteric lymph nodes (Figure 5K).

CD8^{+} lymphocytes use the secretion of granzyme B (GZMB) and perforin as a primary mechanism to induce cell killing. Once released, perforin destroys the cell membrane, allowing the GZMB to be delivered to target cells and exert its pro-apoptotic function. IFN-γ, produced by both CD8^{+} and CD4^{+} T lymphocytes, synergistically acts with GZMB and perforin to induce apoptosis and to further stimulate the anti-tumor immune response[57,58].

This pattern was confirmed by qPCR analysis, in which GZMB and IFN-γ resulted upregulated at the transcriptional level, paralleled by an increased expression of CXCL9 and CXCL10 chemokines (Figure 5L), whose role is related to T cells recruitment[59]. Collectively, these data suggested that CD300e deficiency is associated to an effective anti-tumor response established through to the modulation of macrophages' functional profile which in turn promotes a T cell-mediated anti-tumor response.

CD300e expressing macrophages support tumor growth

To define whether the inhibition tumor growth specifically depended on the lack of CD300e on macrophages, we perform an adoptive transfer of TAM. BMDMs from CD300e$^{-/-}$ and CD300e$^{+/+}$ mice were differentiated with macrophage colony-stimulating factor (M-CSF) and stimulated *in vitro* with IL-4 to induce a TAM phenotype; TAMs were then injected in CD300e$^{+/+}$ mice in a 1:3 ratio with MC38 cells (Figure 6A). CD300e$^{+/+}$-derived TAMs accelerated the tumor growth of MC38 cells, whereas depletion of CD300e attenuated the tumor-promoting role of TAMs (Figure 6B). Despite no significant differences were detected in terms of monocytes and macrophages overall infiltrate (Figure 6D), the relative proportion of macrophages highly expressing MHC-II and MHC-I were

significantly increased in mice inoculated with CD300e$^{-/-}$ TAMs, while macrophages expressing PD-L1 was reduced in the same mice (Figure 6E). Similarly, the tumor-infiltrating lymphocytes analysis recapitulated what observed in MC38 CD300e$^{-/-}$-bearing mice, with an increased activated T cells infiltration (Figure 6F). Finally, the analysis of local lymph node T cells confirmed a higher proportion of IFN-γ producing CD4^{+} and CD8^{+} T cells in MC38 CD300e$^{+/+}$-bearing mice inoculated with CD300e$^{-/-}$ TAM (Figure 5G). Overall, these results confirm, indeed, that CD300e expressing TAM are responsible for generating a tumor-promoting immune environment

.

Discussion

CD300e is a relatively understudied immune receptor belonging to the CD300 family of receptors, initially identified as an immune activating molecule whose expression is restricted to myeloid cell lineages[26,29]. Recent findings highlighted a potential immunoregulatory function of the receptor in monocytes and macrophages[25,30]; however, connection of CD300e in remodeling the monocytes/macrophages functional profile and the tumor immune microenvironment has never been investigated yet. Here, our findings indicate that the immune receptor CD300e significantly shapes the functional profile of TAMs in CRC, fostering a pro-tumorigenic environment that supports tumor progression. The high expression of CD300e in TAMs from CRC patients, which correlates with a marked downregulation of MHC-II expression, suggests that CD300e may play a role in immune evasion by reducing antigen presentation. The shift toward an immunosuppressive phenotype, with increased expression of immunosuppressive molecule CD206 and elevated production of tumor-promotin cytokines such as IL-10 and TGF-β, further supports the notion that CD300e contributes to immune suppression within the TME. This is consistent with other studies highlighting the dual role of TAMs in cancer where they may exhibit a spectrum of polarization states, depending on stimuli exposition in TME, either supporting or inhibiting tumor growth depending on their polarization state[60]. In colorectal cancer, a high infiltration of macrophages has usually been associated to a better prognoisis[61,62], although contradictory reports exist[63,64].

The in vitro co-culture experiments with tumor colon organoids and monocyte-derived macrophages confirmed that the CRC microenvironment can induce CD300e expression, which in turn drives the immunosuppressive and pro-tumor profile of TAMs. Interestingly, CD300e-deficient macrophages displayed enhanced pro-inflammatory activity, including increased expression of MHC-II and other pro-inflammatory markers, alongside an increased capacity for phagocytosis and decreased efferocytosis. These results show that CD300e can upregulate the pro-tumorigenic

cytokines expression and reduce the phagocytosis, thus enhancing the pro-tumorigenic function of macrophages in the tumor microenvironment. These findings are supported by previous studies indicating that macrophages in the TME can be reprogrammed to support tumor growth through similar mechanisms[65].

In vivo, the role of CD300e was further validated in a colitis-associated colorectal cancer model and in a subcutaneous model. CD300e-deficient mice showed reduced tumor burden and increased survival rates compared to wild-type controls. The reduction in tumor growth was associated with a more robust anti-tumor immune response, as evidenced by the increased infiltration of activated CD4+ and CD8+ T cells producing IFN-γ, a cytokine known to enhance anti-tumor immunity. These observations suggest that targeting CD300e could disrupt the immunosuppressive environment maintained by TAMs, thereby enhancing the efficacy of the anti-tumor immune response.

The specific role of CD300e-expressing TAMs in supporting tumor growth has been demonstrated by adoptively transfer of CD300e$^{-/-}$ tumor infiltrating macrophages. Mice receiving CD300e-deficient TAMs exhibited reduced tumor progression, reinforcing the notion that CD300e expression on macrophages is a key driver of their tumor-promoting activity. Our findings aligns with the broader literature on TAMs, which has identified these cells as critical contributors to tumor progression through their support of immunosuppressive environments and promotion of tumor cell survival and metastasis[9,10,24].

In conclusion, this study provides new insights into the immunoregulatory functions of CD300e in the context of CRC. The receptor's role in promoting an immunosuppressive TAM phenotype and supporting tumor progression makes it a promising target for novel therapeutic strategies aimed at enhancing anti-tumor immunity in CRC. By inhibiting CD300e, it may be possible to reprogram TAMs to support anti-tumor immunity rather than tumor progression.

Future studies should focus on developing CD300e inhibitors and evaluating their potential in combination with existing immunotherapies to improve outcomes for CRC patients.

Data availability

All the datasets used and/or analyzed during this study are available from the corresponding author on reasonable request.

Acknowledgement

This work was supported by AIRC MFAG 23192 to GC.

We thank Prof. Vincenzo Bronte from the Veneto Institute of Oncology, Padua, Italy and Prof. Ilaria Marigo from Department of Surgical, Oncological and Gastroenterological Sciences (DiSCOG), University of Padua, Padua, Italy for kindly providing MC38 cell line.

We thank Javier Martin Gonzalez and Rafael Oliveira Brandão from Transgenic Core Facility of the University of Copenhagen for the generation of the CD300e KO mouse.

Authors contribution

G.C. conceptually planned and supervised the study. G.C., A.B. and S.V. designed experiments. A.B. and S.V. performed most of the experiments unless specified. G.C., A.B., S.V., L.M. N.G., S.L., M.B. and E.C. analyzed data. A.B., S.V., S.C., S.G. and S.P. participated in the animal studies. A.B., S.V., F.M., S.G., G.N. and S.C. participated in the molecular and cellular biological experiments. S.L., M.B., M.F. and W.V. helped the pathology-related studies. G.C. and A.B. wrote the manuscript. G.S., M.F. and W.V. participated in the clinical sample and information collection. G.S. conceptualized clinical aspects and contributed to clinical sample collection and data analysis. All authors have read and approved the manuscript.

Declaration of interest

No conflict of interest

Supporting information

Supplementary figures are included in the present version of the manuscript.

References

1. Arnold, M. *et al.* Global patterns and trends in colorectal cancer incidence and mortality. *Gut* **66**, 683–691 (2017).
2. Siegel, R. L., Giaquinto, A. N. & Jemal, A. Cancer statistics, 2024. *CA A Cancer J Clinicians* **74**, 12–49 (2024).
3. Li, J., Chen, D. & Shen, M. Tumor Microenvironment Shapes Colorectal Cancer Progression, Metastasis, and Treatment Responses. *Front. Med.* **9**, 869010 (2022).
4. Peddareddigari, V. G., Wang, D. & DuBois, R. N. The Tumor Microenvironment in Colorectal Carcinogenesis. *Cancer Microenvironment* **3**, 149–166 (2010).
5. Kather, J. N. & Halama, N. Harnessing the innate immune system and local immunological microenvironment to treat colorectal cancer. *Br J Cancer* **120**, 871–882 (2019).
6. Guo, L., Wang, C., Qiu, X., Pu, X. & Chang, P. Colorectal Cancer Immune Infiltrates: Significance in Patient Prognosis and Immunotherapeutic Efficacy. *Front. Immunol.* **11**, 1052 (2020).
7. Pagès, F. *et al.* International validation of the consensus Immunoscore for the classification of colon cancer: a prognostic and accuracy study. *Lancet (London, England)* **391**, 2128–2139 (2018).
8. Galon, J. *et al.* Cancer classification using the Immunoscore: a worldwide task force. *J Transl Med* **10**, 205 (2012).
9. Hourani, T. *et al.* Tumor Associated Macrophages: Origin, Recruitment, Phenotypic Diversity, and Targeting. *Front. Oncol.* **11**, 788365 (2021).
10. Bied, M., Ho, W. W., Ginhoux, F. & Blériot, C. Roles of macrophages in tumor development: a spatiotemporal perspective. *Cell Mol Immunol* **20**, 983–992 (2023).
11. Franklin, R. A. *et al.* The cellular and molecular origin of tumor-associated macrophages. *Science* **344**, 921–925 (2014).

12. Li, X., Chen, L., Peng, X. & Zhan, X. Progress of tumor-associated macrophages in the epithelial-mesenchymal transition of tumor. *Front. Oncol.* **12**, 911410 (2022).
13. Thiery, J. P., Acloque, H., Huang, R. Y. J. & Nieto, M. A. Epithelial-Mesenchymal Transitions in Development and Disease. *Cell* **139**, 871–890 (2009).
14. Dongre, A. & Weinberg, R. A. New insights into the mechanisms of epithelial–mesenchymal transition and implications for cancer. *Nat Rev Mol Cell Biol* **20**, 69–84 (2019).
15. Bonde, A.-K., Tischler, V., Kumar, S., Soltermann, A. & Schwendener, R. A. Intratumoral macrophages contribute to epithelial-mesenchymal transition in solid tumors. *BMC Cancer* **12**, 35 (2012).
16. Huang, R., Kang, T. & Chen, S. The role of tumor-associated macrophages in tumor immune evasion. *J Cancer Res Clin Oncol* **150**, 238 (2024).
17. Cassetta, L. & Kitamura, T. Macrophage targeting: opening new possibilities for cancer immunotherapy. *Immunology* **155**, 285–293 (2018).
18. Cheng, N., Bai, X., Shu, Y., Ahmad, O. & Shen, P. Targeting tumor-associated macrophages as an antitumor strategy. *Biochemical Pharmacology* **183**, 114354 (2021).
19. Zhong, X., Chen, B. & Yang, Z. The Role of Tumor-Associated Macrophages in Colorectal Carcinoma Progression. *Cellular physiology and biochemistry : international journal of experimental cellular physiology, biochemistry, and pharmacology* **45**, 356–365 (2018).
20. Pinto, M. L. *et al.* The Two Faces of Tumor-Associated Macrophages and Their Clinical Significance in Colorectal Cancer. *Front. Immunol.* **10**, 1875 (2019).
21. Kumari, N. & Choi, S. H. Tumor-associated macrophages in cancer: recent advancements in cancer nanoimmunotherapies. *J Exp Clin Cancer Res* **41**, 68 (2022).
22. Li, Y. *et al.* Functional and Therapeutic Significance of Tumor-Associated Macrophages in Colorectal Cancer. *Front. Oncol.* **12**, 781233 (2022).

23. Gordon, S. R. *et al.* PD-1 expression by tumour-associated macrophages inhibits phagocytosis and tumour immunity. *Nature* **545**, 495–499 (2017).
24. Zhang, Y., Zhao, Y., Li, Q. & Wang, Y. Macrophages, as a Promising Strategy to Targeted Treatment for Colorectal Cancer Metastasis in Tumor Immune Microenvironment. *Front. Immunol.* **12**, 685978 (2021).
25. Pagliari, M. *et al.* Helicobacter pylori Affects the Antigen Presentation Activity of Macrophages Modulating the Expression of the Immune Receptor CD300E through miR-4270. *Front. Immunol.* **8**, 1288 (2017).
26. Isobe, M. *et al.* The CD300e molecule in mice is an immune-activating receptor. *Journal of Biological Chemistry* **293**, 3793–3805 (2018).
27. Aguilar, H. *et al.* Molecular characterization of a novel immune receptor restricted to the monocytic lineage. *Journal of immunology (Baltimore, Md. : 1950)* **173**, 6703–6711 (2004).
28. Zenarruzabeitia, O. *et al.* The expression and function of human CD300 receptors on blood circulating mononuclear cells are distinct in neonates and adults. *Sci Rep* **6**, 32693 (2016).
29. Brckalo, T. *et al.* Functional analysis of the CD300e receptor in human monocytes and myeloid dendritic cells. *Eur. J. Immunol.* **40**, 722–732 (2010).
30. Coletta, S. *et al.* The immune receptor CD300e negatively regulates T cell activation by impairing the STAT1-dependent antigen presentation. *Sci Rep* **10**, 16501 (2020).
31. Hamidzadeh, K., Belew, A. T., El-Sayed, N. M. & Mosser, D. M. The transition of M-CSF–derived human macrophages to a growth-promoting phenotype. *Blood Advances* **4**, 5460–5472 (2020).
32. Adamczyk, A. M. *et al.* Extracellular vesicles from human plasma dampen inflammation and promote tissue repair functions in macrophages. *J of Extracellular Vesicle* **12**, 12331 (2023).
33. Uhlen, M. *et al.* Proteomics. Tissue-based map of the human proteome. *Science* **347**, 1260419–1260419 (2015).

34. Luo, Z. *et al.* Exercise-downregulated CD300E acted as a negative prognostic implication and tumor-promoted role in pan-cancer. *Front. Immunol.* **15**, 1437068 (2024).

35. Shang, S. *et al.* ID1 expressing macrophages support cancer cell stemness and limit CD8+ T cell infiltration in colorectal cancer. *Nat Commun* **14**, 7661 (2023).

36. Sato, T. *et al.* Long-term expansion of epithelial organoids from human colon, adenoma, adenocarcinoma, and Barrett's epithelium. *Gastroenterology* **141**, 1762–1772 (2011).

37. Noel, G. *et al.* A primary human macrophage-enteroid co-culture model to investigate mucosal gut physiology and host-pathogen interactions. *Sci Rep* **7**, 45270 (2017).

38. D'Elios, M. M. *et al.* The Helicobacter cinaedi antigen CAIP participates in atherosclerotic inflammation by promoting the differentiation of macrophages in foam cells. *Sci Rep* **7**, 40515 (2017).

39. Vallese, F. *et al.* Helicobacter pylori antigenic Lpp20 is a structural homologue of Tipα and promotes epithelial-mesenchymal transition. *Biochimica et Biophysica Acta (BBA) - General Subjects* **1861**, 3263–3271 (2017).

40. Li, B. & Dewey, C. N. RSEM: accurate transcript quantification from RNA-Seq data with or without a reference genome. *BMC Bioinformatics* **12**, 323 (2011).

41. Yu, G., Wang, L.-G., Han, Y. & He, Q.-Y. clusterProfiler: an R Package for Comparing Biological Themes Among Gene Clusters. *OMICS: A Journal of Integrative Biology* **16**, 284–287 (2012).

42. Wu, T. *et al.* clusterProfiler 4.0: A universal enrichment tool for interpreting omics data. *The Innovation* **2**, 100141 (2021).

43. Uhlén, M. *et al.* A Human Protein Atlas for Normal and Cancer Tissues Based on Antibody Proteomics. *Molecular & Cellular Proteomics* **4**, 1920–1932 (2005).

44. Lee, H.-O. *et al.* Lineage-dependent gene expression programs influence the immune landscape of colorectal cancer. *Nat Genet* **52**, 594–603 (2020).

45. Coletta, S. *et al.* Tumor Cells and the Extracellular Matrix Dictate the Pro-Tumoral Profile of Macrophages in CRC. *Cancers (Basel)* **13**, 5199 (2021).
46. Lavender, N. *et al.* The Yin/Yan of CCL2: a minor role in neutrophil anti-tumor activity in vitro but a major role on the outgrowth of metastatic breast cancer lesions in the lung in vivo. *BMC Cancer* **17**, 88 (2017).
47. Molgora, M. *et al.* TREM2 Modulation Remodels the Tumor Myeloid Landscape Enhancing Anti-PD-1 Immunotherapy. *Cell* **182**, 886-900.e17 (2020).
48. Zhang, M., Li, X., Zhang, Q., Yang, J. & Liu, G. Roles of macrophages on ulcerative colitis and colitis-associated colorectal cancer. *Front. Immunol.* **14**, 1103617 (2023).
49. Zhou, X., Liu, X. & Huang, L. Macrophage-Mediated Tumor Cell Phagocytosis: Opportunity for Nanomedicine Intervention. *Adv Funct Materials* **31**, 2006220 (2021).
50. Biswas, S. K. & Mantovani, A. Macrophage plasticity and interaction with lymphocyte subsets: cancer as a paradigm. *Nat Immunol* **11**, 889–896 (2010).
51. DeNardo, D. G. & Ruffell, B. Macrophages as regulators of tumour immunity and immunotherapy. *Nat Rev Immunol* **19**, 369–382 (2019).
52. Doran, A. C., Yurdagul, A. & Tabas, I. Efferocytosis in health and disease. *Nat Rev Immunol* **20**, 254–267 (2020).
53. Zhou, Y. *et al.* Blockade of the Phagocytic Receptor MerTK on Tumor-Associated Macrophages Enhances P2X7R-Dependent STING Activation by Tumor-Derived cGAMP. *Immunity* **52**, 357-373.e9 (2020).
54. Feng, M. *et al.* Phagocytosis checkpoints as new targets for cancer immunotherapy. *Nat Rev Cancer* **19**, 568–586 (2019).

55. Parang, B., Barrett, C. W. & Williams, C. S. AOM/DSS Model of Colitis-Associated Cancer. in *Gastrointestinal Physiology and Diseases* (ed. Ivanov, A. I.) vol. 1422 297–307 (Springer New York, New York, NY, 2016).

56. Rashidian, M. *et al.* Immuno-PET identifies the myeloid compartment as a key contributor to the outcome of the antitumor response under PD-1 blockade. *Proc. Natl. Acad. Sci. U.S.A.* **116**, 16971–16980 (2019).

57. Metkar, S. S. *et al.* Human and Mouse Granzyme A Induce a Proinflammatory Cytokine Response. *Immunity* **29**, 720–733 (2008).

58. Hay, Z. L. Z. & Slansky, J. E. Granzymes: The Molecular Executors of Immune-Mediated Cytotoxicity. *IJMS* **23**, 1833 (2022).

59. Dangaj, D. *et al.* Cooperation between Constitutive and Inducible Chemokines Enables T Cell Engraftment and Immune Attack in Solid Tumors. *Cancer Cell* **35**, 885-900.e10 (2019).

60. Guerriero, J. L. Macrophages: The Road Less Traveled, Changing Anticancer Therapy. *Trends in Molecular Medicine* **24**, 472–489 (2018).

61. Koelzer, V. H. *et al.* Phenotyping of tumor-associated macrophages in colorectal cancer: Impact on single cell invasion (tumor budding) and clinicopathological outcome. *OncoImmunology* **5**, e1106677 (2016).

62. Forssell, J. *et al.* High Macrophage Infiltration along the Tumor Front Correlates with Improved Survival in Colon Cancer. *Clin Cancer Res* **13**, 1472–1479 (2007).

63. Kim, Y. *et al.* The distribution of intratumoral macrophages correlates with molecular phenotypes and impacts prognosis in colorectal carcinoma. *Histopathology* **73**, 663–671 (2018).

64. Feng, Q. *et al.* Tumor-associated Macrophages as Prognostic and Predictive Biomarkers for Postoperative Adjuvant Chemotherapy in Patients with Stage II Colon Cancer. *Clinical Cancer Research* **25**, 3896–3907 (2019).

65. Kloosterman, D. J. & Akkari, L. Macrophages at the interface of the co-evolving cancer ecosystem. *Cell* **186**, 1627–1651 (2023).

Figure legends

Figure 1. CD300e is expressed by tumor-associated macrophages in CRC and is upregulated in the tumor context. A) CD300e total content was evaluated by Western blot in matched NM and CRC tissue. Blot refers to three representative CRC patients (P1, P2, and P3). Quantification of CD300e was performed by densitometry and normalized to Vinculin as housekeeping protein. Data are expressed as *n*-fold of matched CRC *vs* NM tissue (mean ± SD of 8 CRC patients). **B-D**) mRNA expression of CD300e (B), MHC-II (**C**) and CIITA (**D**) was evaluated in matched NM and CRC tissue by qRT-PCR. Data were normalized to β-actin as an endogenous reference gene and are expressed as $2^{-\Delta\Delta Ct}$ of CRC tissue relative to matched NM tissue (mean ± SD of 6 CRC patients). **E**) Representative images from NM and CRC samples sequentially immunostained for MHC-II (red) and CD163 (blue)/CD300e (brown). Arrows highlight CD300e^{+}/MHC-II^{low} macrophages. The histogram shows the percentage of CD300e^{+}/MHC-II^{low} macrophages in NM and CRC tissue expressed as mean ± SD of 8 CRC patients. **F**) Scheme of normal colon organoid (NCO) and tumor colon organoid (TCO) generation from CRC patients' tissue (upper panel) and of the co-culture between NCO or TCO with monocytes derived from healthy donors (lower panel). The image has been created with Biorender. **G**) Surface expression and mRNA expression of CD300e were evaluated by flow cytometry and qRT-PCR, respectively, on monocyte-derived macrophages after 5 d of co-culture with either NCO or TCO. Surface expression is expressed as n-fold vs macrophages co-cultured with NCO ± SD. mRNA expression was normalized on β-actin as an endogenous reference gene and is expressed as $2^{-\Delta\Delta Ct}$ relative to monocyte-derived macrophages cultured with NCO, ± SD (n = 4 different monocyte donors co-cultured with 4 NCO and 4 TCO lines). **H**) The surface expression of MHC-II, CD86, and CD206 was evaluated by flow cytometry on monocyte-derived macrophages after 5 d of co-culture with either NCO or TCO. Data are expressed as n-fold vs macrophages co-cultured with NCO ± SD of the experiments in **G**). **I**) mRNA expression of CD163, CD206, IL-10, IL-6, and TGF-β was evaluated

on macrophages after 5 d of co-culture as in **H**). Data were normalized on β-actin as an endogenous reference gene and expressed as $2^{-\Delta\Delta Ct}$ relative to macrophages co-cultured with NCO, ± SD of the experiments in **G**). **J**) Release of IL-6 and IL-10 in the co-culture supernatants collected after 5 d of co-culture of macrophages with either NCO or TCO by ELISA assay. Data are expressed as n-fold vs supernatants of macrophages co-cultured with NCO ± SD of the experiments in **G**). Statistical significance was determined by Student's t-test. CRC = colorectal cancer; NM = normal colonic mucosa; NCO = normal colon organoids; TCO = tumor colon organoids. *=p≤0.05; **= p≤0.01; ***=p≤0.001; ****=p≤0.0001.

Figure 2. CD300e$^{-/-}$ macrophages co-cultured with tumor colon organoids acquire an immunostimulatory and phagocytic profile. A) mRNA expression of CD300e and MHC-II was evaluated by qRT-PCR in murine macrophages before (t0) and after 48 hours of co-culture with tumor colon organoids (+ TCO). Data were normalized on β-actin and 18S and as endogenous reference genes and are expressed as $2^{-\Delta\Delta Ct}$ relative to macrophages at t0 (mean ± SD, n = 6 CD300e$^{+/+}$ macrophage donors co-cultured with 3 different TCO lines). B) The mRNA expression of macrophage immunostimulatory (CD38, CD86, iNOS, MHC-II, TNF-α) and immunosuppressive (EGR2, CD163, CD206, Arginase1, TGF-β) markers was evaluated by qRT-PCR on CD300e$^{+/+}$ and CD300e$^{-/-}$ macrophages after 48 hours of co-culture with TCO. Data were normalized on β-actin and 18S and as endogenous reference genes and are expressed as $2^{-\Delta\Delta Ct}$ relative to CD300e$^{+/+}$ macrophages (mean ± SD of 9 CD300e$^{+/+}$ and 9 CD300e$^{-/-}$ macrophage donors, co-cultured with 3 different TCO lines). **C**) After 48 hours of co-culture with TCO, macrophages were incubated for 30 minutes with Zymosan A BioParticles™ to evaluate their phagocytic ability. Representative confocal images of CD300e$^{+/+}$ and CD300e$^{-/-}$ macrophages ± Cytocalasin D are shown. Nuclei are stained with DAPI (blue), F4/80 was used as macrophage marker (green) and Zymosan BioParticles™ are visualized in red. Scale bar = 50 µm. The number of internalized Zymosan A BioParticles™ was

manually counted; data are expressed as ratio of the number of Zymosan A BioParticles on the number of phagocytic macrophages (macrophages that internalized ≥1 bioparticle) of 3 CD300e$^{+/+}$ and 3 CD300e$^{-/-}$ macrophage donors exposed to 2 different TCO lines. Ten images per condition were analyzed. **D,E**) After 48 hours of co-culture with TCO, macrophages were incubated for 2 hours with live MC38 cells (**D**) or 1 hour with apoptotic MC38 cells (**E**) to evaluate their capacity to phagocytose live (phagocytosis) or apoptotic (efferocytosis) tumor cells. Confocal images represent macrophages stained with Vybrant DiO (green) and MC38 cells stained with Vybrant DiD (red). Scale bar = 50 µm. The percentage of macrophages that phagocytosed MC38 cells was manually calculated on seven images per condition (n = 3 CD300e+/+ and 3 CD300e-/- macrophage donors). Statistical significance was determined by Student's t-test. CytD = Cytocalasin D; NT = untreated; TCO = tumor colon organoids. *=p≤0.05; **= p≤0.01; ****=p≤0.0001.

Figure 3. The lack of CD300e in macrophages decreases the induction of EMT-related genes and improves epithelial integrity in tumor colon organoids. A) mRNA expression of a panel of genes related to epithelial to mesenchymal transition (EMT) evaluated by qRT-PCR on tumor colon organoids (TCO) after 48 hours of co-culture with either CD300e**+/+** or CD300e**-/-** macrophages. Data were normalized on β-actin and 18S and as endogenous reference genes and are expressed as $2^{-\Delta\Delta Ct}$ relative to TCO co-cultured with CD300e$^{+/+}$ macrophages (mean ± SD of 3 different TCO lines co-cultured with 9 CD300e$^{+/+}$ and 9 CD300e$^{-/-}$ macrophage donors. **B**) Permeability of intestinal organoids, after 48 hours of co-culture with macrophages, measured after 1h incubation with FITC-dextran, 4 kDa. Representative confocal images of TCO co-cultured with CD300e$^{+/+}$ and CD300e$^{-/-}$ macrophages are shown. Scale bar = 100 µm. FITC fluorescence intensity was measured inside organoid lumen and normalized on background fluorescence. Histogram represents mean fluorescence ratio ± SD of 2 TCO lines co-cultured with 2 CD300e$^{+/+}$ and 2 CD300e$^{-/-}$ macrophage donors (≥ 10 organoids per condition were analyzed). **C**) Scheme of the 2D co-culture between TCO-

derived monolayers and macrophages on a Transwell insert (left). After 48 hours of co-culture with CD300e$^{+/+}$ or CD300e$^{-/-}$ macrophages, TCO-derived monolayers were incubated for 1 hour with FITC-dextran, 4kDa in the top compartment of Transwell systems, and FITC fluorescence was measured in the bottom compartment. Data are expressed as *n*-fold relative to TCO-derived monolayers exposed to CD300e$^{+/+}$ macrophages (middle). Transepithelial electrical resistance was measured across TCO-derived monolayers after 48 hours of co-culture with macrophages. Data are expressed as n-fold relative to TCO-derived monolayers exposed to CD300e$^{+/+}$ macrophages (right). Histograms represent mean ± SD of 2 different TCO lines co-cultured with 3 CD300e$^{+/+}$ and 3 CD300e$^{-/-}$ macrophage donors. EMT = epithelial to mesenchymal transition; FITC = fluoresceine isothiocyanate; TEER = transepithelial electrical resistance; TCO = tumor colon organoids. Statistical significance was determined by Student's t test. *p≤0.05; **p≤0.01; ****=p≤0.0001.

Figure 4. CD300e$^{-/-}$ mice develop a lower tumor burden and display an improved anti-tumor immune response upon AOM/DSS treatment. A) The weight of mice undergoing AOM/DSS treatment was recorded throughout the experimental period (90 days). Mice weights at all time points are expressed as percentage of the weight at the beginning of the experiment (day 0, before AOM injection), ± SD (n = 16 CD300e+/+ and 14 CD300e-/- mice). **B**) Kaplan-Meier survival analysis was conducted on AOM/DSS-treated mice (n = 16 CD300e$^{+/+}$ and 14 CD300e$^{-/-}$ mice). **C**) Colon length was measured after sacrifice at the end of AOM/DSS treatment. Representative pictures of colons of CD300e$^{+/+}$ and CD300e$^{-/-}$ mice are shown. Histogram represents colon lengths expressed as mean ± SD o 16 CD300e$^{+/+}$ and 14 CD300e$^{-/-}$ mice. **D**) Representative pictures of longitudinally opened colons of CD300e$^{+/+}$ and CD300e$^{-/-}$ mice after AOM/DSS treatment are shown (left). Once colons were opened, the number of tumors was counted (left histogram) and the area of each tumor was approximately measured (right histogram) as d1xd2, being d1 and d2 the major and minor dimensions of each tumor. The sum of tumor areas was calculated for each mouse and expressed

as total area per mouse. Histograms represent mean ± SD (n = 16 CD300e$^{+/+}$ and 14 CD300e$^{-/-}$ mice). **E**) mRNA expression of Arginase1, CD206, IL-6, and IL-1β was evaluated by qRT-PCR on colonic tumor tissue of AOM/DSS treated mice. Data were normalized on β-actin and 18S and as endogenous reference genes and are expressed as $2^{-\Delta\Delta Ct}$ relative to CD300e$^{+/+}$ mice (mean ± SD of 3 CD300e$^{+/+}$ and 3 CD300e$^{-/-}$ mice). F) The production of IFN-γ was evaluated in mesenteric lymph nodes of AOM/DSS treated mice. After overnight non-specific activation of mesenteric lymphocytes, IFN-γ levels were measured by flow cytometry. Data are expressed as percentage of IFN-γ-positive CD4^{+} (left) and CD8^{+} (right) T lymphocytes (mean ± SD of 9 CD300e$^{+/+}$ and 9 CD300e$^{-/-}$ mice). Statistical significance was determined by Student's t test. AOM = azoxymethane; DSS = dextran sodium sulfate. *p≤0.05; **p≤0.01; ***=p≤0.001.

Figure 5. CD300e ablation delays MC38 tumor growth and modifies the tumor-immune infiltrate. **A**) Growth kinetics of MC38 colon adenocarcinoma in mice (mean ± SD of n = 8 CD300e$^{+/+}$ and 10 CD300e$^{-/-}$ mice). Šídák's multiple comparisons test: ****p≤0.0001. B) Representative pictures of excised tumors are shown (left). Tumors were weighed (middle) and the final volume (right) was determined. **C-E**) CD11b^{+} myeloid cells (gated on CD3^{-}CD19^{-}NK1.1^{-}CD11b^{+} cells) were identified as Ly6G^{+}Ly6C^{+} neutrophils (**C**), Ly6G^{-}Ly6C^{+} monocytes (**D**) and F4/80^{+}CD11c^{+} macrophages (**E**). **F**) Representative histograms of MHC-II, MHC-I, and PD-L1 surface expression in tumor-infiltrated macrophages. Data are expressed as mean fluorescence intensity (MFI) ± SD (n = 5 CD300e$^{+/+}$ and 7 CD300e$^{-/-}$ mice). **G**) CD4^{+} and CD8^{+} T lymphocytes populations (gated on CD11b^{-}CD3^{+} cells) were evaluated in tumor immune infiltrates. **H**) Representative histograms of PD-1 surface expression in tumor-infiltrated CD4+ and CD8^{+} T cells. Data are expressed as mean fluorescence intensity (MFI) ± SD (n = 5 CD300e$^{+/+}$ and 7 CD300e$^{-/-}$ mice). I) GZMB and Perforin expression by tumor-infiltrating lymphocytes was measured by flow cytometry. Data are expressed as percentage of GZMB- and Perforine-positive CD8+ T cells (mean ± SD of 8 CD300e$^{+/+}$ and 10 CD300e$^{-/-}$ mice). **J**) IFN-γ

production by tumor-infiltrating lymphocytes was measured by flow cytometry. Data are expressed as percentage of IFN-γ-positive $CD4^+$ (left) and $CD8^+$ (right) T lymphocytes (mean ± SD of 8 $CD300e^{+/+}$ and 10 $CD300e^{-/-}$ mice). **K**) IFN-γ production by lymphocytes in the draining lymph node of MC38 tumor-bearing mice (mean ± SD of 8 $CD300e^{+/+}$ and 10 $CD300e^{-/-}$ mice). L) mRNA expression of GZMB, IFN-γ, CXCL9 and CXCL10 was evaluated by qRT-PCR on dissociated tumor tissues. Data were normalized on β-actin and 18S and as endogenous reference genes and are expressed as $2^{-\Delta\Delta Ct}$ relative to $CD300e^{+/+}$ mice (mean ± SD of 8 $CD300e^{+/+}$ and 10 $CD300e^{-/-}$ mice). Statistical significance was determined by Student's t test. *p≤0.05; **p≤0.01; ****p≤0.0001.

Figure 6. CD300e-depleted macrophages counteract tumor development and impact tumor myeloid and lymphoid landscape. BMDMs obtained from $CD300e^{+/+}$ and $CD300e^{-/-}$ mice were stimulated in vitro with IL-4 to induce a TAM phenotype, mixed with MC38 cells, and adoptively transferred into $CD300e^{+/+}$ recipient mice. **A**) Schematic diagram of macrophage adoptive transfer model based on the s.c. injection of MC38-TAMs-like BMDMs mixture. Created with Biorender. **B**) Growth kinetics of MC38 tumors in injected mice (mean ± SD of n = 3 $CD300e^{+/+}$ and 3 $CD300e^{-/-}$ TAMs-transplanted mice). C) Representative pictures of tumors are shown in the left part of the panel; tumor weight and volume are shown in the right part of the panel (mean ± SD). **D**) The percentage of $Ly6C^+$ monocytes and $F4/80^+$ macrophages were evaluated in the tumors of TAMs-transplanted mice. Data are expressed as cell percentage (%) on $CD3^-CD19^-NK1.1^-$ cells (mean ± SD). **E**) Representative histograms of MHC-II, MHC-I, and PD-L1 surface expression in tumor-infiltrated macrophages (expressed as mean fluorescence intensity (MFI) ± SD). **F**) The frequency of $CD4^+$ and $CD8^+$ infiltrating T lymphocytes was determined in tumor immune infiltrates from $CD300e^{+/+}$ and $CD300e^{-/-}$ mice. Data are expressed as cell percentage (%) on $CD11b^-$ cells (mean ± SD). G) The production of IFN-γ was evaluated by flow cytometry in local lymph nodes after an overnight non-specific activation of lymphocytes. Data are expressed as percentage of IFN-γ-positive $CD4^+$ (left)

and $CD8^+$ (right) T lymphocytes (mean ± SD of n = 3 $CD300e^{+/+}$ and 3 $CD300e^{-/-}$ TAMs-transplanted mice). Statistical significance was determined by Student's t test. *$p \leq 0.05$; **$p \leq 0.01$

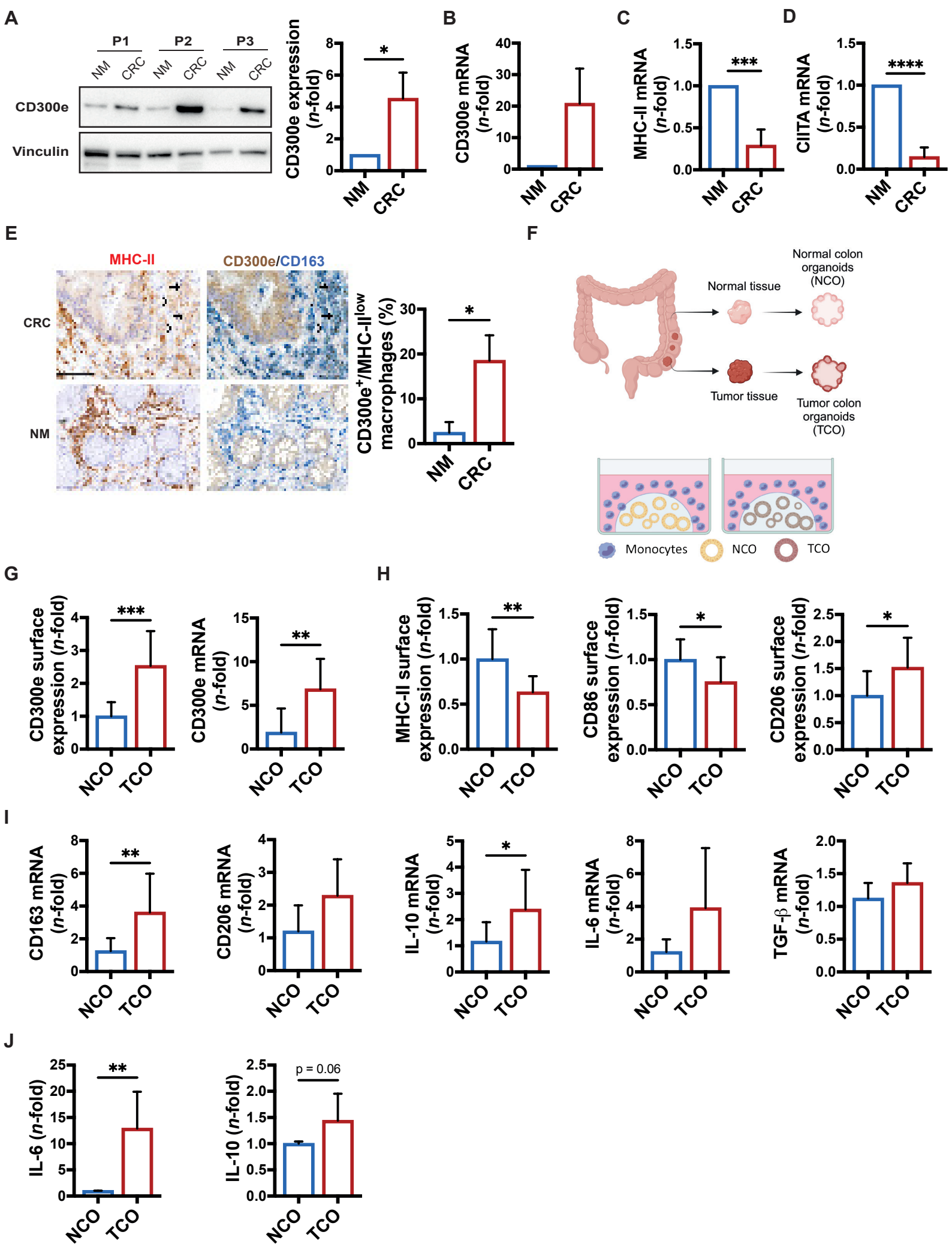
A
P1
P2
P3
NM
CRC
CD300e
Vinculin
CD300e expression (n-fold)
B
CD300e mRNA (n-fold)
C
MHC-II mRNA (n-fold)
CIITA mRNA (n-fold)
D
E
MHC-II
CD300e/CD163
CRC
NM
CD300e+/MHC-IIlow macrophages (%)
F
Normal tissue
Normal colon organoids (NCO)
Tumor tissue
Tumor colon organoids (TCO)
Monocytes
NCO
TCO
G
CD300e surface expression (n-fold)
CD300e mRNA (n-fold)
H
MHC-II surface expression (n-fold)
CD86 surface expression (n-fold)
CD206 surface expression (n-fold)
I
CD163 mRNA (n-fold)
CD206 mRNA (n-fold)
IL-10 mRNA (n-fold)
IL-6 mRNA (n-fold)
TGF-β mRNA (n-fold)
J
IL-6 (n-fold)
IL-10 (n-fold)
p = 0.06

Figure 1

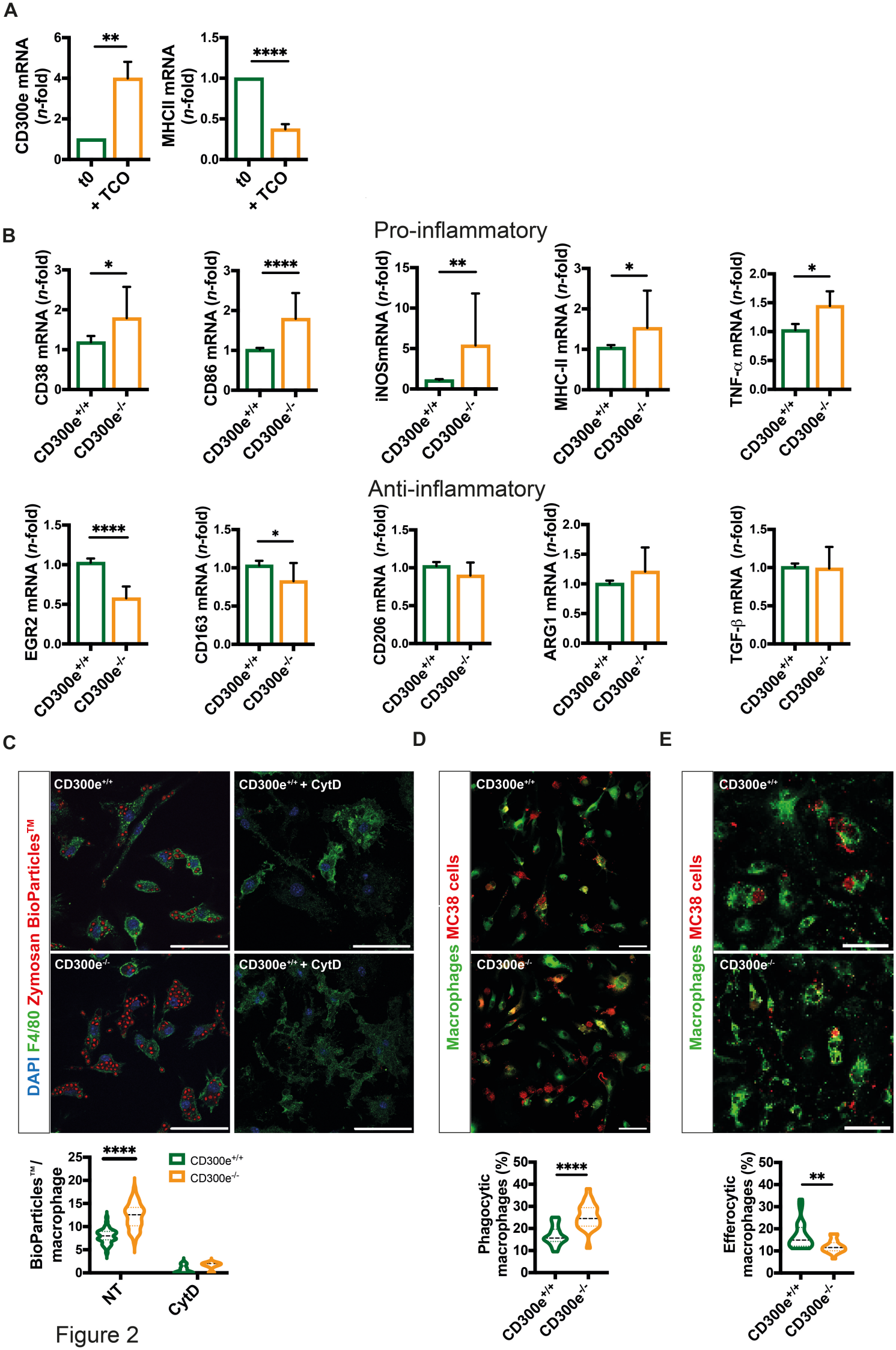
A
CD300e mRNA (n-fold)
MHCII mRNA (n-fold)
t0
+ TCO
B
Pro-inflammatory
CD38 mRNA (n-fold)
CD86 mRNA (n-fold)
iNOSmRNA (n-fold)
MHC-II mRNA (n-fold)
TNF-α mRNA (n-fold)
CD300e+/+
CD300e-/-
Anti-inflammatory
EGR2 mRNA (n-fold)
CD163 mRNA (n-fold)
CD206 mRNA (n-fold)
ARG1 mRNA (n-fold)
TGF-β mRNA (n-fold)
C
D
E
DAPI F4/80 Zymosan BioParticles™
CD300e+/+
CD300e+/+ + CytD
CD300e-/-
Macrophages MC38 cells
BioParticles™ / macrophage
NT
CytD
Phagocytic macrophages (%)
Efferocytic macrophages (%)

Figure 2

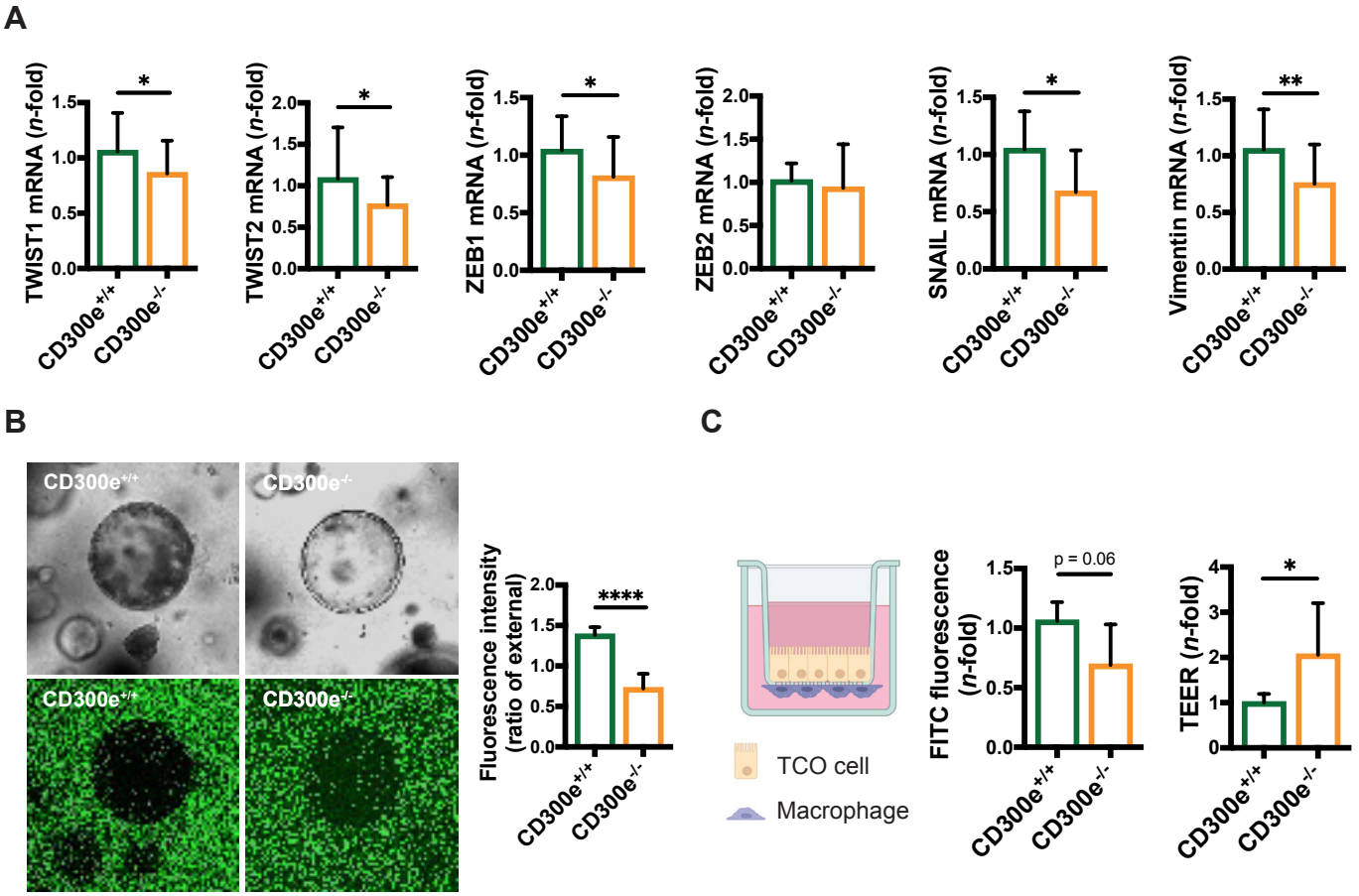
A
TWIST1 mRNA (n-fold)
TWIST2 mRNA (n-fold)
ZEB1 mRNA (n-fold)
ZEB2 mRNA (n-fold)
SNAIL mRNA (n-fold)
Vimentin mRNA (n-fold)
CD300e+/+
CD300e-/-
B
Fluorescence intensity (ratio of external)
****
C
TCO cell
Macrophage
FITC fluorescence (n-fold)
p = 0.06
TEER (n-fold)

Figure 3

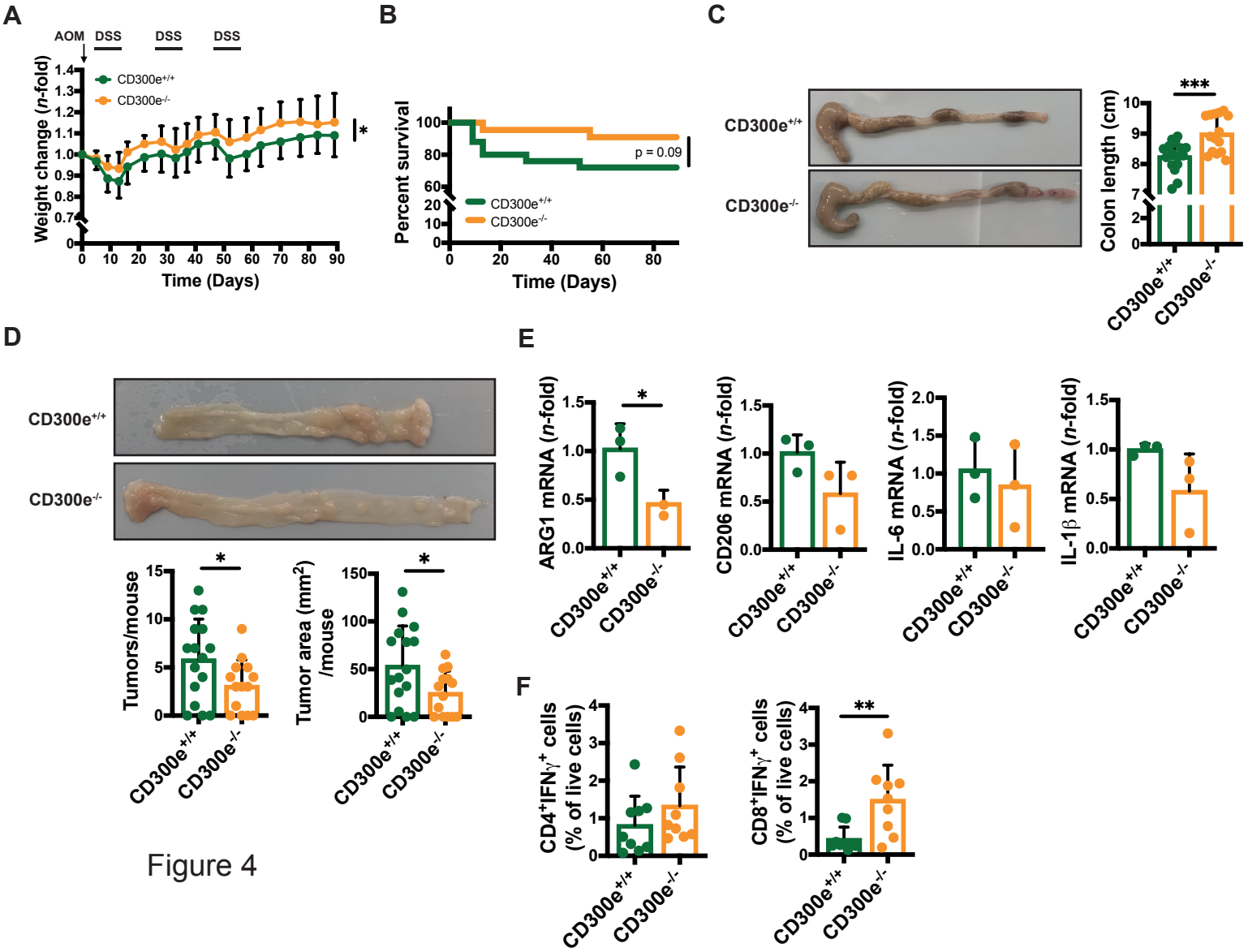
A
AOM
DSS
DSS
DSS
Weight change (n-fold)
CD300e+/+
CD300e-/-
Time (Days)
*
B
Percent survival
p = 0.09
CD300e+/+
CD300e-/-
Time (Days)
C
CD300e+/+
CD300e-/-
Colon length (cm)
***
D
CD300e+/+
CD300e-/-
Tumors/mouse
Tumor area (mm2) /mouse
E
ARG1 mRNA (n-fold)
CD206 mRNA (n-fold)
IL-6 mRNA (n-fold)
IL-1β mRNA (n-fold)
F
CD4+IFNγ+ cells (% of live cells)
CD8+IFNγ+ cells (% of live cells)
**

Figure 4

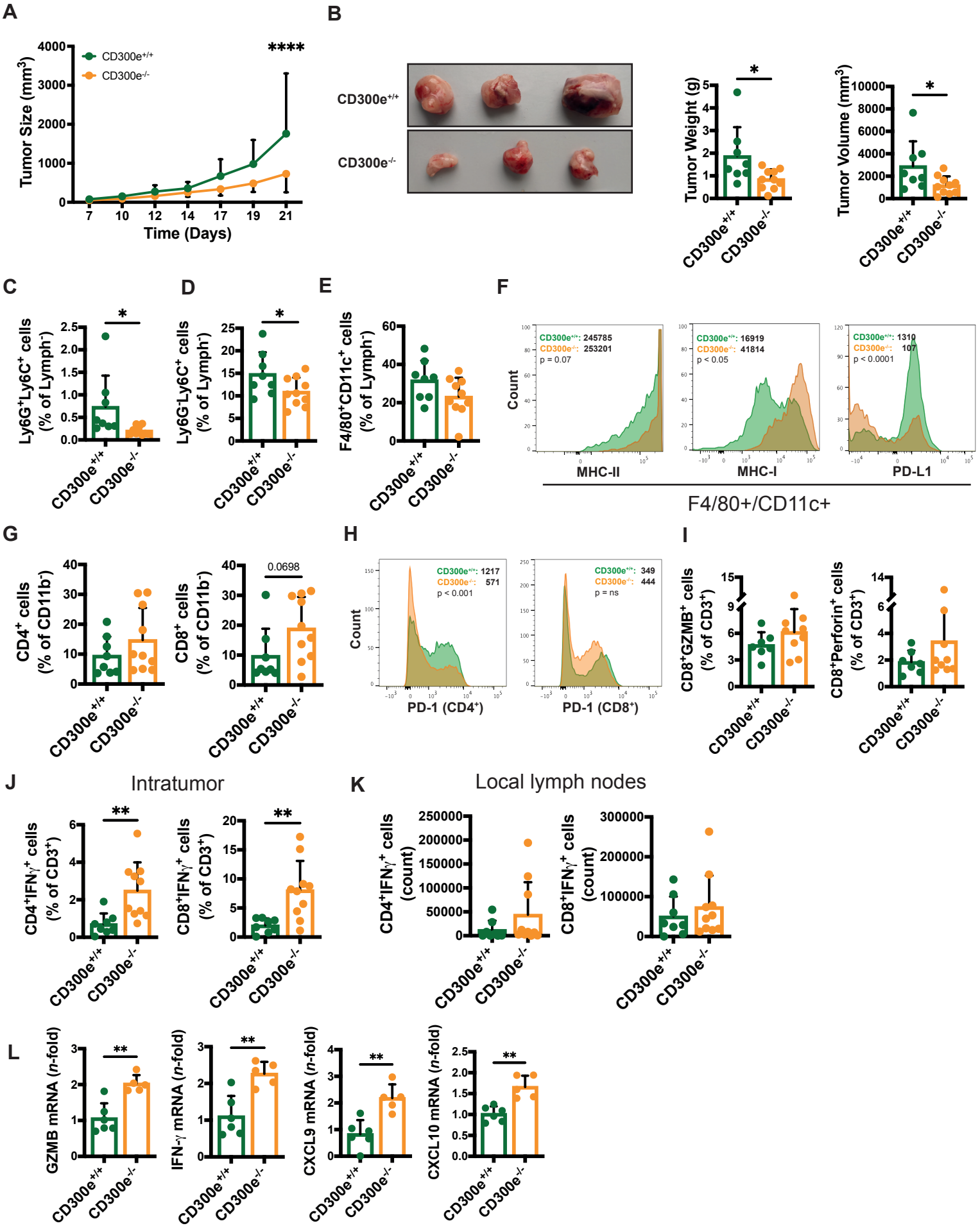
A
Tumor Size (mm³)
CD300e+/+
CD300e-/-
****
Time (Days)
B
CD300e+/+
CD300e-/-
Tumor Weight (g)
Tumor Volume (mm³)
C
Ly6G+Ly6C+ cells (% of Lymph-)
D
Ly6G-Ly6C+ cells (% of Lymph-)
E
F4/80+CD11c+ cells (% of Lymph-)
F
Count
CD300e+/+: 245785
CD300e-/-: 253201
p = 0.07
CD300e+/+: 16919
CD300e-/-: 41814
p < 0.05
CD300e+/+: 1310
CD300e-/-: 107
p < 0.0001
MHC-II
MHC-I
PD-L1
F4/80+/CD11c+
G
CD4+ cells (% of CD11b-)
CD8+ cells (% of CD11b-)
0.0698
H
CD300e+/+: 1217
CD300e-/-: 571
p < 0.001
CD300e+/+: 349
CD300e-/-: 444
p = ns
PD-1 (CD4+)
PD-1 (CD8+)
I
CD8+GZMB+ cells (% of CD3+)
CD8+Perforin+ cells (% of CD3+)
J
Intratumor
CD4+IFNγ+ cells (% of CD3+)
CD8+IFNγ+ cells (% of CD3+)
K
Local lymph nodes
CD4+IFNγ+ cells (count)
CD8+IFNγ+ cells (count)
L
GZMB mRNA (n-fold)
IFN-γ mRNA (n-fold)
CXCL9 mRNA (n-fold)
CXCL10 mRNA (n-fold)

Figure 5

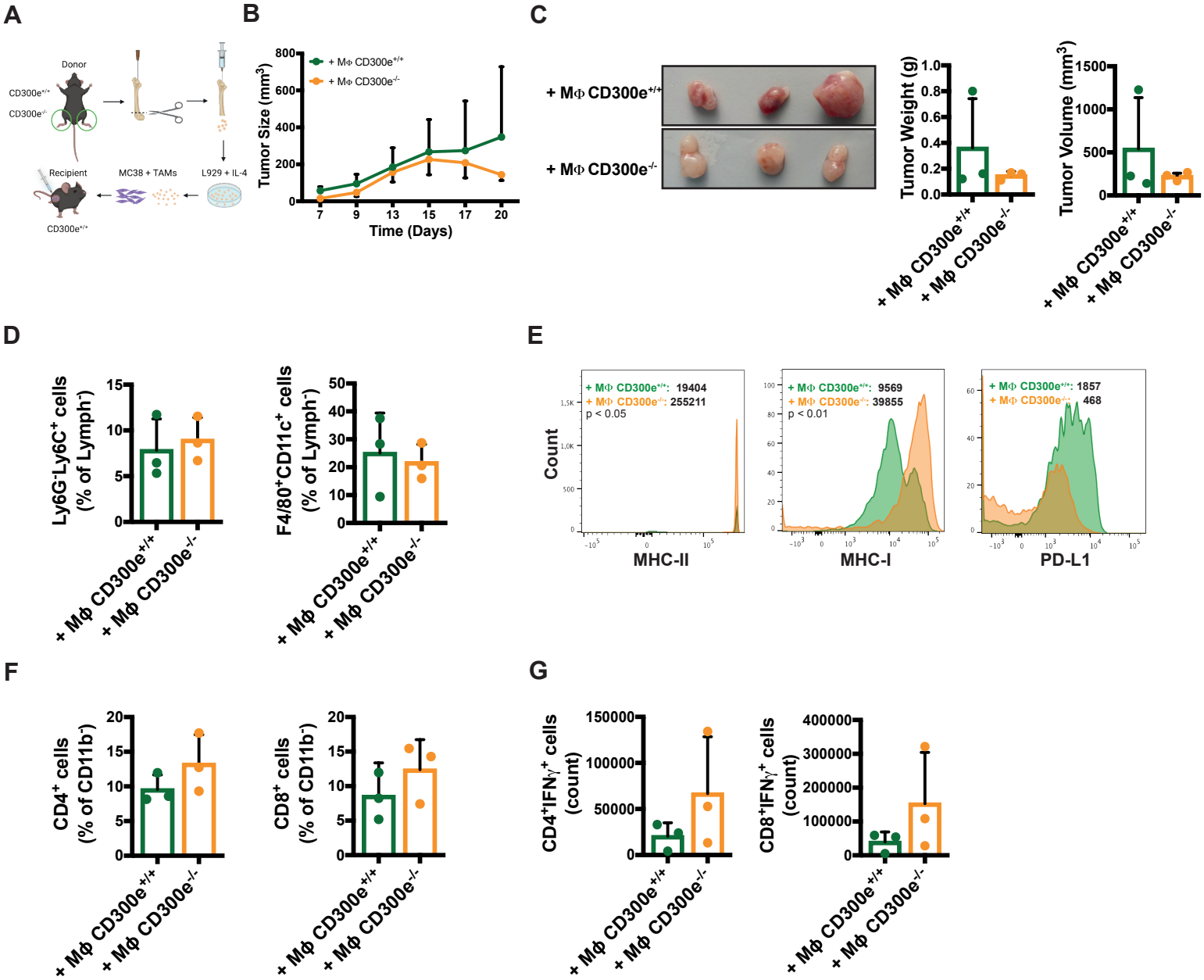
A
Donor
CD300e+/+
CD300e-/-
Recipient
CD300e+/+
MC38 + TAMs
L929 + IL-4
B
+ MΦ CD300e+/+
+ MΦ CD300e-/-
Tumor Size (mm3)
Time (Days)
C
+ MΦ CD300e+/+
+ MΦ CD300e-/-
Tumor Weight (g)
Tumor Volume (mm3)
D
Ly6G-Ly6C+ cells (% of Lymph-)
F4/80+CD11c+ cells (% of Lymph-)
E
+ MΦ CD300e+/+: 19404
+ MΦ CD300e-/-: 255211
p < 0.05
+ MΦ CD300e+/+: 9569
+ MΦ CD300e-/-: 39855
p < 0.01
+ MΦ CD300e+/+: 1857
+ MΦ CD300e-/-: 468
Count
MHC-II
MHC-I
PD-L1
F
CD4+ cells (% of CD11b-)
CD8+ cells (% of CD11b-)
G
CD4+IFNγ+ cells (count)
CD8+IFNγ+ cells (count)

Figure 6